
SAHLGRENSKA ACADEMY

# Automatic exposure control for digital radiography without a physical anti-scatter grid

Master's thesis in Medical Physics

Louise Ring
**Department of Medical radiation sciences**
UNIVERSITY OF GOTHENBURG
Gothenburg, Sweden 2025

Master's thesis 2025

# Automatic exposure control for digital radiography without a physical anti-scatter grid

Louise Ring


UNIVERSITY OF GOTHENBURG

Sahlgrenska academy
*Institute of Clinical Sciences*
Department of Medical radiation sciences
University of Gothenburg
Gothenburg, Sweden 2025

Automatic exposure control for digital radiography without a physical anti-scatter grid
Louise Ring



Supervisors:

Patrik Sund, Ph. D., Department of Medical Physics and Biomedical Engineering, Sahlgrenska University Hospital, Gothenburg, Sweden, and Department of Medical Radiation Sciences, Institute of Clinical Sciences, Sahlgrenska Academy, University of Gothenburg, Gothenburg, Sweden.

Maria Hultenmo, M. Sc., Department of Medical Physics and Biomedical Engineering, Sahlgrenska University Hospital, Gothenburg, Sweden

Dieudonne Daba, M. Sc., Department of Medical Physics and Biomedical Engineering, Sahlgrenska University Hospital, Gothenburg, Sweden

Examiner:

Magnus Båth, Professor, Medical radiation sciences, Institute of clinical sciences, Sahlgrenska academy, University of Gothenburg.

Master's Thesis 2025
Institute of Clinical Sciences
Department of Medical radiation sciences
University of Gothenburg
Gula stråket 2B SU/Sahlgrenska
SE-41345 Gothenburg

Typeset in LaTeX
Gothenburg, Sweden 2025

A University of Gothenburg Master's thesis
Louise Ring
Department of Medical radiation sciences
University of Gothenburg

# Abstract

*Purpose:* This study aimed to find a factor $R$ for different parameter settings that can be used to adjust the AEC preset value, in order to maintain a constant amount of primary radiation to the detector when the anti-scatter grid is removed. *Method and materials:* A factor $R$ was calculated as the fraction between dose-area product (DAP) with and without an anti-scatter grid, from each exposure on polymethylmethacrylate (PMMA) phantoms, multiplied with a primary transmission factor $T_p$. These measurements lead to a deeper understanding of how varying PMMA thickness, kV and field size would influence $R$. Second, anthropomorphic phantoms were examined, with a built-in AEC assistance detector (BiAA), while increasing their thicknesses and using different kV and field sizes. An adult chest phantom were examined in anteroposterior (AP) and lateral (LAT) projections (AP/LAT thickness: 21/29, 27/35, 32/39 cm). An adult pelvis and hip phantom (thickness: 23, 29, 35 cm) was examined in AP projection. A pediatric chest phantom (thickness: 15 cm) was examined in AP projection. *Results:* The $R$s from examination of the PMMA resulted in an increase as the thickness increased. This trend was also observed when the field size increased. However, as the kV increased, $R$ decreased. The adult chest (thickness: 21, 27 and 32 cm) AP examination resulted in $R$s of 1.13, 1.36 and 1.59. The adult chest (thickness: 29, 35, 39 cm) LAT examination resulted in $R$s of 1.20, 1.36 and 1.51, with 141 kV. The adult pelvis (thickness: 23, 29, 35 cm) AP examination resulted in $R$s of 2.89, 3.49 and 4.13 with 70 kV. The $R$s for the hip examination were 2.34, 2.95 and 2.62. The pediatric chest (thickness: 15 cm) AP examination resulted in an $R$ of 1.08. *Discussion and conclusion:* $R$ had a similar relative increase for the examination of the adult chest and pelvis with increasing thickness, but $R$ was higher for the pelvis. The change in $R$ between the different thicknesses and phantoms was substantial, which implies the importance of optimizing the examination protocol according to patient size during a gridless examination with AEC. The difference in $R$ also means that the protocol should include a combination of $R$ for a specific anatomic region and patient size, for a finer adjustment of the AEC preset dose. The results of the pediatric phantom measurement, where two different mA were used, the lower mA increased the exposure time. However, the exposure time remained shorter than the minimum recommended by the generator manufacturer. This implies that for smaller thicknesses, the AEC may not be reliable. This study can be used as a base for further studies, and the performance of virtual anti-scatter grids and its impact on image quality needs to be investigated.

# Sammanfattning

*Syfte*: Syftet med denna studie var att finna en faktor $R$ för olika parameterinställningar som kan användas för att justera den förinställda AEC-dosen, i syfte att bibehålla en konstant mängd primärstrålning till detektorn när det fysiska rastert tas bort. *Metod och material*: Först beräknades en faktor $R$, från dos-area-produkten (DAP) för AEC exponeringar med och utan ett raster multiplicerat med en primärtransmissions faktor, på flera PMMA-fantom. Dessa mätningar skapade en djupare förståelse om hur varierande PMMA-tjocklek, kV och fältstorlek skulle påverka $R$. För det andra, undersöktes antropomorfa fantom och samtidigt som deras tjocklek ökade, varierade även kV och fältstorlek i mätningarna. Ett vuxen thoraxfantom undersöktes i anterioposterior (AP) och laterala (LAT) projektioner (AP/LAT-tjocklek: 21/29, 27/35, 32/39 cm). Ett vuxen bäcken- och höftfantom (tjocklek: 23, 29, 35 cm) undersöktes i AP-projektion. En pediatrisk thoraxfantom (tjocklek: 15 cm) undersöktes i AP-projektion och med två olika milliampere (mA), 25 och 50 mA. *Resultat*: $R$ från mätningar av PMMA resulterade i en ökning när tjockleken ökade. Denna trend observerades också när fältstorleken ökade. När kV ökade, minskade $R$. AP-undersökning av det vuxna thoraxfantomet (AP-tjocklek: 21, 27 och 32 cm) resulterade i $R$ på 1.13, 1.36 och 1.59, med 125 kV. LAT-undersökningen av det vuxna thoraxfantomet (LAT-tjocklek: 29, 35, 39 cm) resulterade i $R$ på 1.20, 1.36 oh 1.51 med 141 kV. AP-undersökningen för det vuxna bäckenfantomet (tjocklek: 23, 29, 35 cm) resulterade i $R$ på 2.89, 3.49 och 4.13 med 70 kV. $R$ för höftundersökningen var 2.34, 2.95 och 2.62. AP-undersökningen på det pediatriska fantomet (tjocklek: 15 cm) resulterade i $R$ på 1.08. *Diskussion och sammanfattning:* $R$ hade en liknande relativ ökning för undersökningen av det vuxna thoraxfantomet och bäckenfantomet med ökande tjocklek, men $R$ var högre för bäckenet. Förändringen i $R$ mellan de olika tjocklekarna och fantomen var betydande, vilket innebär att optimering av undersökningsprotokollet utifrån patientstorlek innan en undersökning, utan fysiskt raster, är viktigt. Skillnaden i $R$ innebär också att protokollet bör innehålla en kombination av $R$ för en specifik anatomisk region och patientstorlek, för en finare justering av AEC-dosen. Resultatet från mätningen med det pediatriska fantomet, där två olika mA-inställningar användes, visade att den lägre mA-nivån ökade exponeringstiden. Exponeringstiden var dock fortfarande kortare än den minimitid som rekommenderas av tillverkaren av generatorn. Detta antyder att AEC kanske inte är tillförlitlig vid mindre kroppstjocklekar. Denna studie kan användas som grund för vidare forskning, och prestandan hos virtuella antistrålningsgaller samt deras inverkan på bildkvaliteten behöver undersökas.

Keywords: Anti-scatter grid, PMMA, anthropomorphic phantom, built-in AEC detector

# Acknowledgments

Firstly, I would like to thank my supervisors, Patrik Sund, Maria Hultenmo and Dieudonne Daba, for their support, guidance and feedback. This study would not be possible without them. I would also like to thank Mediel AB for letting me cooperate and use their latest radiological equipment. I have learned a lot during this study process, which I am forever thankful for. To all the people who supported me emotionally during this study, you have my deepest gratitude, especially my family and my fiancé, Emir Bosnic, and my dear friends Albin, Alexander and Emma.

Louise Ring, Gothenburg, January 2025

# Contents

# List of Figures

# List of Tables

# 1

# Introduction

Digital radiography is a common diagnostic procedure for the examination of the body and is used to diagnose various diseases, e.g. cancer, for guidance during surgery, or to visualize the tissues inside the body (Cancerfonden, 2023). A digital radiography system has a source, where X-ray radiation is produced, and a digital detector. When the primary radiation passes through a patient's body, some of the radiation will scatter in to different directions and some radiation will be absorbed in the patient. The amount of radiation that will travel straight through the patient decreases due to scattered and absorbed radiation. The detector receives both the radiation that travels straight through the patient and some of the scattered radiation. Optimally, the X-ray image contains the difference between the radiation going through the patient and the absorbed and scattered radiation. However, scattered radiation that reaches the detector can result in a decreased image quality (Sayed et al., 2023).

There are different parameters that contribute to a change in scattered radiation, for example, tube voltage, field size of the irradiated area, and patient thickness (Ghafarian et al., 2007). In many examinations, the use of an anti-scatter grid in front of a detector is common. The scattered radiation as well as the primary radiation are being reduced from entering the digital detector, but the scattered radiation is reduced to a greater extent, resulting in an increased portion of the primary radiation. The anti-scatter grid can result in better image quality when used properly (Verstreepen et al., 2023).

A preset dose is set in the system before examination and when the dose reaches the limit the exposure stops. This system is called automatic exposure control (AEC) and it adjusts the exposure time for different patient sizes. The AEC is often used to examine the chest and abdomen. The dose in AEC systems can be measured with ionization chambers that are often placed in front of the digital detector, however, there are detectors today that have AEC built-in to the detector which enables quicker read out of the received signal (Canon Inc., 2021). This also makes it possible for a new era with a portable radiography system, that has not existed before.

An advantage of digital radiography is that it can be mobile/portable and directly after the examination the image can be viewed. This is a benefit for the assessment of patients who are unwell and have difficulties moving, like bedside examinations at intensive care units. For these patients, quick imaging is critical, which means that the anti-scatter grid needs to be placed correctly, and if not it could increase

the radiation dose, because of the high risk of re-examination (Verstreepen et al., 2023). Newer technology can reduce the effect of scattered radiation in the image by using a software, without having the limitations of the physical anti-scatter grid and improving the image quality, known as a virtual anti-scatter grid. One benefit of eliminating the usage of the physical anti-scatter grid is the reduced patient dose, another benefit is that removing the grid from an examination will omit a misplaced grid. On the other hand, excluding the grid can reduce the contrast in the medical images, which is often a dilemma in pediatric radiography (Fritz and Jones, 2014). Another challenge with removing the physical grid is the scattered radiation that enters the AEC and stops the exposure prematurely. However, the physical grid reduces both the scattered and primary radiation, and by removing the physical grid, the primary radiation will no longer be reduced. Therefore, the patient dose can be decreased.

## 1.1 Aims of the study

This study aimed to find a factor $R$ for different parameter settings that can be used to adjust the AEC preset value, in order to maintain a constant amount of primary radiation to the detector when the anti-scatter grid is removed. The effects of varying kV, thicknesses, and field sizes during PMMA phantom exposures were examined, and $R$ was evaluated. Also, three anthropomorphic phantoms were examined with a BiAA detector, with and without an anti-scatter grid.

# 2

# Theory

## 2.1 Conventional radiography

### 2.1.1 Radiation physics

Radiography is a method that uses X-ray beams to obtain an internal image of a patient's body for cancer diagnostics or other medical examinations common in hospitals. An X-ray tube consists of the following main components: an electron source (a tube cathode), an anode/target, and a glass envelope (Dance et al., 2014). The electrons are produced in a filament, a larger current will create more electrons in the filament, and the current will be expressed as milliamperes (mA). To create X-ray radiation, the electrons need to be accelerated and collide with the target on the anode, the acceleration occurs when a potential is applied over the cathode and anode. The potential is regulated by the tube voltage (kV). Allowing exposure with a set mA for a period of exposure time (s) is referred to as tube load (mAs). The exposure time, tube voltage, and tube current are all important but different exposure parameters. The kV and the mAs affect the quality and quantity of the X-ray beam, as a change in kV is a change in photon energy and a change in both kV and mAs changes the amount of created photons, i.e the amount of radiation. The fourth main component, the glass envelope, contains and surrounds all of the other components.

The created X-ray beam consists of two types of radiation, Bremsstrahlung and characteristic radiation (Dance et al., 2014, chapter 5). The Bremsstrahlung radiation consists of a wide range of energies, created by the retardations of electrons by the force near the nucleus. The characteristic radiation consists of one energy, created by an electron colliding into another one in the atomic shell and ejecting it from the atom. An X-ray photon is emitted as an electron de-excites from one atomic shell to another, and the energy of that photon is equal to the energy difference between those shells. The majority of the radiation energy in the X-ray beam consists of Bremsstrahlung radiation.

As the radiation exits the envelope, there are other components that control the size of the beam and change the X-ray energy spectrum. Collimators form the field size by blocking the distal part of the X-ray beam, reducing the beam creates a smaller field. By inserting a filter, the lower energies in the beam spectrum will be reduced or attenuated which is preferable (Dance et al., 2014, chapter 5). The low energy photons would attenuate or scatter in a patient's body, resulting in increased patient

dose.

Before an examination of a patient, the exposure parameters as kV, mA, and field size are set based on the body part and patient anatomy. However, if an AEC is used, the exposure time is automatically controlled by the AEC and the exposure stops when a certain dose limit is reached (Dance et al., 2014, chapter 5). The exposure parameters affect the radiation dose to the patient and the AEC does not change the fact that a suitable kV, mA, or field size must be chosen for a successful examination. Therefore, the parameter needs to be chosen with caution or the image can be under- or overexposed, which may lead to poor image quality or unnecessary radiation dose to the patient. This implies that the exposure parameters must be chosen to ensure the image contains diagnostic information, meaning the radiation must be limited.

Scattered radiation occurs when the radiation interacts with matter, such as a patient's tissues, and its appearance could reduce the diagnostic value in the obtained image. The degree of scattered radiation can increase with the patient's thickness and the density of the exposed matter (Sy et al., 2024).

To prevent the scattered radiation from entering the detector, an anti-scatter grid can be used. The grid has the purpose of limiting the scattered radiation at the same time as allowing the primary radiation to pass and enter the detector (Dance et al., 2014, chapter 6).

There are several types of digital detectors in radiography and a frequently used detector is a flat-panel detector. Using either a scintillator or photoconductor layer, the X-rays translate to an electric signal with the help of a thin-film transistor (Lança and Silva, 2009). One of the latest detectors on the market is a digital detector that has a built-in AEC system inside the detector (Canon Inc, 2023).

### 2.1.2 Tube output measurement

Dose-area product (DAP) is one parameter that can be analyzed after an examination. DAP is defined as the radiation dose to air (Gy) multiplied with the field size ($cm^2$), resulting in a unit of e.g $Gycm^2$. The radiation dose to air can be measured with a DAP-meter, in many radiography systems, which is placed after/underneath the collimators in the X-ray tube. DAP represents how much radiation dose that has been delivered during the exposure.

Another exposure parameter is the tube load (mAs). An increase in mAs will increase the mA or exposure time and that will increase the amount of radiation exiting the X-ray tube. In fact, an increase in the mAs will lead to an increase in radiation dose to the patient and is linearly related to the DAP value. Therefore the mAs provided at the exposure is one way to understand the amount of radiation given to the patient, since the increased mAs corresponds to an increased radiation dose (Sy et al., 2024).

### 2.1.3 Anti-scatter grid

Scattered radiation constantly appears when exposing patients, regardless of patient size. The resulting image quality is often degraded by the scattered radiation. Thickness, kV and field size are three parameters that affect the scattered radiation. By increasing the field size, kV and thickness, the amount of scattered radiation increases (Ghafarian et al., 2007). To reduce the amount of scattered radiation registered by the detector, an anti-scatter grid can be placed between the patient and the image detector.

An anti-scatter grid is designed with lead strips. One characteristic of a grid is measured as grid ratio $r$,

$$r = \frac{h}{d} \tag{2.1}$$

where $h$ is the height of the lead strips and $d$ is the distance between the lead strips (Dance et al., 2014). The ratio is often written as h:d. Another important property is strip frequency $f$, $\text{cm}^{-1}$, which is how many lead strips that occur per centimetre. An additional property for an anti-scatter grid is the primary transmission, $T_p$, that represents the amount of primary radiation transmitted through the grid. $T_p$ is calculated by the fraction between the dose obtained with and without the anti-scatter grid, ideally using only primary radiation without any contribution from scattered radiation.

Between the lead strips is an interspacer, a material that is less attenuating, for example plastic. The purpose of the lead is to attenuate the scattered radiation and only the primary radiation that goes through the interspacer should pass and register in the detector, see Figure 2.1 (Dance et al., 2014, chapter 6.3.4).

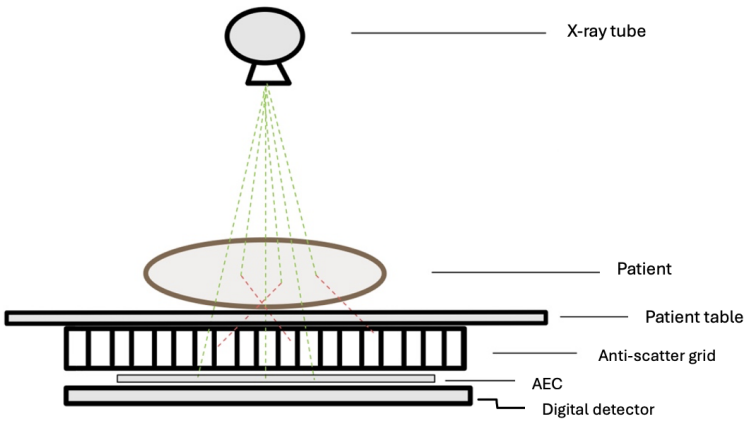


**Figure 2.1:** Schematic figure of the usage of an anti-scatter grid. From the X-ray tube the primary radiation (green) can go through the patient and the anti-scatter grid to the detector. The primary radiation can also scatter (red) in the object or patient on a patient table, as seen in the figure, and then be attenuated or absorbed by the anti-scatter grid, which is illustrated as the thin black lines under the patient table in the figure.

Every grid has what is called a focal length, it is the recommended distance where the field divergence and the grid align to accept the majority of the primary radiation to pass through but not the scattered. If a grid is placed at a length greater or smaller than the focal length, then the primary radiation will attenuate in the lead strips, this is a concept called grid cut-off (Dance et al., 2014, chapter 6). The grid cut-off is also caused by a tilted grid or by a decentred grid.

Due to the fact that the anti-scatter grid needs to be placed correctly, some examinations such as bedside examinations can cause grid cut-off. In bedside examinations, it can be time-consuming and difficult to place the grid correctly, since both the X-ray tube, the grid and the detector are manually positioned. In addition, the grid can be heavy which makes it difficult to operate. If the obtained images appear to be non-diagnostic, multiple exposures will be needed. This can not only make the patients more uncomfortable, but also receive an increased radiation dose. This is one reason for why the grid can be excluded for some examinations, with the benefit of reducing the patient dose (Ahn et al., 2018). The anti-scatter grid does not only reduce the scattered radiation, but also the primary radiation. Consequently, the radiation exposure needs to increase when the grid is used (Dance et al., 2014, chapter 6). Therefore, the increased radiation results in a higher radiation dose.

Younger patients are typically examined without an anti-scatter grid and manually installed exposure settings, since thin patients do not contribute to a lot of scattered radiation (Sayed et al., 2023). Region Västra Götaland has a method book for adult chest examination in their county, it is recommended to use an anti-scatter grid when examining both in anterior-posterior and lateral views (Sanna Axelsson, 2023). The grid is not recommended when the patient weighs under 20 kg.

### 2.1.4 Virtual anti-scatter grid

The latest invention regarding scatter reduction is a virtual anti-scatter grid, which is an algorithm. The algorithm varies between manufacturers, but is based on the same method. Pre-existing models for radiation attenuation through different material are used to obtain data on how much scattered radiation is in the pixel values in the exposed images. This scattered radiation is then subtracted from the pixel values, resulting in a clearer image (Sayed et al., 2023). When the physical grid is replaced with the virtual grid, the ability to physically stop the scattered radiation is lost which makes it possible for the primary and scattered radiation to reach the AEC and detector.

### 2.1.5 Automatic exposure control

In radiology, a digital detector receives radiation and creates an image, the detector itself is not usually involved in adjusting the exposure. The AEC is an independent system that will control the exposure. The number of AEC-regions varies but the most common is three regions, two side chambers and one central chamber, and it can be chosen which region is active during exposure.

The purpose of AEC is to adjust the exposure time as the exposure is ongoing. The main benefit of AEC is that it helps when the patient size differs because the image

quality for diagnostics must be relatively equal, therefore it adjusts the exposure parameters (IAEA, 2024).

AEC can be combined with physical anti-scatter grids. But the virtual grid like the one from Philips is recommended to be used with manual/free exposure settings (Philips, 2015), and not combined with the AEC. This is most likely true for all virtual grids.

Some radiography systems have dose-level steps, called density control (Dance et al., 2014). These steps can adjust the exposure. By increasing or decreasing the density steps, the radiation dose increase or decrease by around 20%. Radiography systems have the density step 0 as its origin, which refers to a specific radiation dose to the AEC set by the manufacturer. The radiographer can change the exposure by choosing another density.

### 2.1.6 Exposure Index

One exposure indicator is the exposure index (EI), which provides information about the detector exposure due to the signal made from the radiation (Seibert and Morin, 2011). To help technicians, EI is used as an indicator of image quality and to evaluate the correct usage of the radiation equipment for each examination. The EI is a measure of the detector signal obtained from the radiation that reaches the detector, both primary and scattered radiation. The EI-value inform the technician if a suitable dose was given. EI does not represent patient dose and manufacturers define EI differently, which makes the EI vary and should not be compared between manufacturers without understanding the different methods (Seibert and Morin, 2011).

Before the digitalization of detectors, screen-film was used in radiology (Rosa et al., 2024). By studying the screen-film after examination, one could tell if the film was over- or underexposed, but with digital detectors it is the EI that tells this information (Seibert and Morin, 2011).

### 2.1.7 Anti-scatter grid: radiation dose vs image quality

According to Almén (2020) the radiation dose in conventional radiography, for adults in Sweden, has been reduced since the year 2005 because of various reasons, such as the development of digital detectors. One example is the radiation dose for standing lung examination, which has been reduced from 0.38 $\text{Gycm}^2$ year 2006 to 0.21 $\text{Gycm}^2$ year 2019.

The dose reduction over the last years can be explained by the advanced technology in radiology. Another possible method for the dose reduction is to remove the grid. A study by Šabič (2016) showed that by removing the anti-scatter grid the patient dose was reduced. The study also discussed that it can even be unnecessary for chest images of pediatric patients up to 40 kg. Another study by Abela et al. (2022) who also analyzed the removal of the anti-scatter grid for adult knee radiography, showed that knee thicknesses 10 and 12 cm the grid could be removed for any examined kV without impairing the image quality. This was also true for 14 cm of

thickness but only when using 80 kV. There have been studies on how the image quality alters when removing the anti-scatter grid. Mekis et al. (2024) showed that for gridless adult cervical spine radiography, the dose decreased. However, the AP projection on the phantom resulted in a decreased objective image quality. The gridless examination with lateral projection barely affected the objective image quality. The study mentioned that more research needed to be done to find the optimal grid settings for this type of examination (Mekis et al., 2024).

The benefit of a gridless examination protocol is the possible dose reduction, but in some situations the image quality may be degraded from this. For example, the examinations of a pelvis, which produces a large amount of scattered radiation because of the thick volume of tissues, may face a challenge with the image quality if a physical grid is removed and replaced with a virtual grid (Precht et al., 2019).

#### 2.1.7.1 Radiation safety

When talking about image quality, the principle of keeping the radiation dose as low as possible, also known as As Low As Reasonably Achievable (ALARA), should be mentioned (Strålsäkerhetsmyndigheten, 2024). The image quality depends on the amount of radiation the detector obtains. Before an examination, the patient's radiation exposure must be justified and optimized (Strålsäkerhetsmyndigheten, 2017). Justification means that the exposure must be more of a benefit than harm for the patient. Optimization means that the radiation dose obtained during an exposure should be kept as low as possible, while still achieving diagnostic image quality.

One important aspect of radiation safety is to examine the patient without an under- or overexposed image, which also means an over or underexposed patient. Before the digital detector when film was in current use, one could distinctly see if the exposure had sufficient dose by the optical density in the image (Gibson and Davidson, 2012). Today, when analyzing an X-ray image with digital detectors the exposure indicators such as EI (see section 2.1.6), can be helpful to evaluate the exposure.

### 2.1.8 The role of the radiographer

Radiographers should oversee the exposure setting before an examination and have some sense of what is appropriate for a specific kind of examination and patient (Dance et al., 2014, chapter 6). Today's digital radiography systems allow a radiographer to choose a patient examination protocol based on the examined body part and then choose a patient size based on the patient's thickness. There are both pros and cons to these systems. The pros are the facilitations of the protocols, it is time-saving not to build every patient protocol, but the cons of forgetting to evaluate the exposure parameters that are automatically installed exist when choosing a protocol and patient size.

The possibility to overexpose patients occurs if the exposure setting is not evaluated before examination and could result in a non-detected overexposure (Seibert and Morin, 2011).

When a patient is examined, the exposure setting should correspond to the patient's anatomy. This involves not only choosing an appropriate kV and mA, but also a suitable field size and exposure time. All these parameters play a key role for the patient's received radiation dose and also the amount of scattered radiation (Ghafarian et al., 2007).

# 3

# Methods

This study was performed in two parts, where the first part was the examination of how the variation of parameters kV, phantom thickness, and field size contributed to scattered radiation when exposing polymethylmethacrylate (PMMA) phantoms using an AEC. A factor, $R$, was calculated and represented the required increase in detector dose, to achieve similar amount of primary radiation to the detector when the anti-scatter grid is removed as when a grid was used. Error propagation was used with the standard deviation in the mean value of the obtained exposures, to compute the uncertainties in $R$, see Appendix 1 Table A.19-A.31. In the second part, exposures on anthropomorphic phantoms with a digital detector with built-in AEC were conducted.

## 3.1 Part 1: Scattered radiation from PMMA

### 3.1.1 Digital radiography system

In the experiments to measure the DAP with and without an anti-scatter grid, the measurements were performed at Sahlgrenska University Hospital, Gothenburg, in one of their radiographic imaging rooms. A radiographic system (T3 Triathlon DR X-Ray System) with a digital detector (Canon: CXDI-401C wireless) was used for every exposure. An anti-scatter grid (JPI Healthcare) was also used, with a grid ratio of 10:1, a strip frequency of 52 lines/cm and a focal distance of 110 cm. In these measurements, the distance between the X-ray tube and the detector was 130 cm. An example of an experimental set-up is shown in Figure 3.1.

### 3.1.2 Phantom

Two different sizes of PMMA phantoms were used to perform the measurements, one was 33 cm wide and 33 cm in length, with a thickness of 1 cm. The other was 25 cm wide, 25 cm in length and 5 cm thick, with a handle on the top of the phantom. Images of the two phantoms can be seen in Figure 3.2. These two different PMMAs were used to construct the desired phantom sizes for the different measurements.

**Figure 3.1:** Photograph of the set-up for the measurements at Sahlgrenska University Hospital. The X-ray tube is located at the top, and the PMMA is placed on the patient table below. Under the table, the anti-scatter grid, AEC, and detector is located.

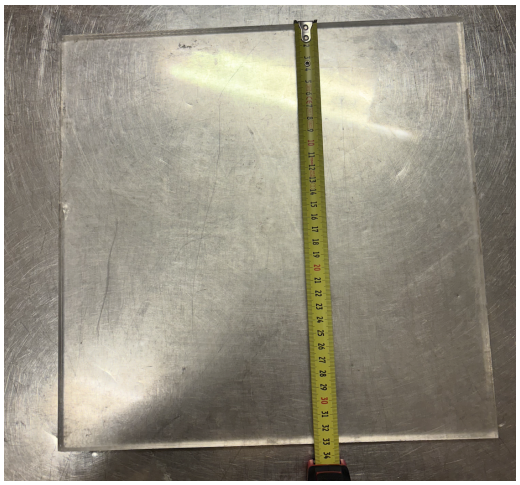

**(a)**

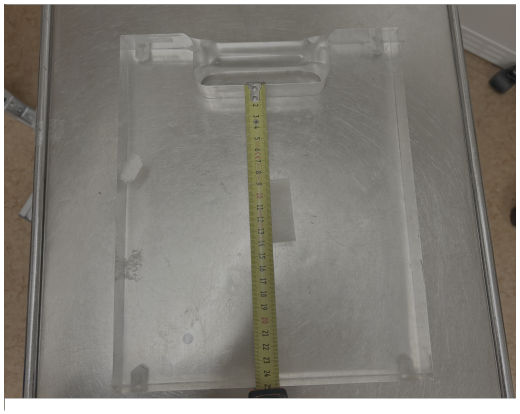

**(b)**

**Figure 3.2:** Images of the PMMA used in the first part of the study. **(a)** A symmetrical PMMA phantom, 33 cm wide and high, with a thickness of 1 cm. **(b)** PMMA phantom, 25 cm wide and high, with a thickness of 5 cm. This phantom also had a handle.

### 3.1.3 Parameter settings

During the measurements, three parameters were varied: the tube voltage, the field size and the thickness of the phantoms. The tube voltage was expressed as kilovolts

(kV) and the thickness of the phantoms in centimeters (cm) in this study. The field size was expressed as "y(cm) x z(cm)" (read as 'y multiplied by z'), and the given field was expressed as the size in the detector plane.

The kV and other exposure settings, such as milliamperes (mA) and filtration, were set manually on a computer in the control room except for the field size. The size of the field was regulated on a panel located on the X-ray tube, with two adjusting handles that had a precision of up to one millimeter.

In the user interface, an examination protocol: frontal pelvis examination on a patient table, was set for all measurements. In that protocol a filtration of 0.1 mm Cu and density of -1 were automatically set. The centre AEC chamber was active for every measurement with the PMMA. Each exposure was performed five times in order to evaluate the reproducibility of the system, both the DAP and mAs were noted.

For every exposure, the persons present were located in the control room, for radiation protection. A short pause was taken between the exposures to be sure that the X-ray tube did not overheat.

#### 3.1.3.1 Varying thickness of the PMMA

The thickness of the PMMA was examined with 80 kV, 400 mA and 20 cm x 20 cm in field size. The thicknesses examined was 10, 12, 15, 17, 20, 22, 25, 27, and 30 cm. The grid was then removed, after five measurement of each thickness, and the same settings where repeated again five consecutive measurements without the grid.

#### 3.1.3.2 Varying the kV

Primarily kV was analysed with an anti-scatter grid and a 10 cm thick PMMA phantom on the patient table, as the exposure settings were set on 500 mA, 50 kV and a field size of 20 cm x 20 cm. The kV then increased from 50 to 60 kV and the phantom was exposed again. This process was repeated, with an increase of 10 kV for each exposure up to 130 kV. The kV influence was examined at different thicknesses: 10, 15, 20, 25, and 30 cm, meaning that each thickness was exposed with 50 up to 130 kV, five times each. After the last measurements, the anti-scatter grid was removed and the same series of settings and phantom thicknesses were examined again.

#### 3.1.3.3 Varying the field size

The field size was examined with 20 cm thick PMMA, as the exposure settings were set on 70 kV, 500 mA and the field size at 15 cm x 15 cm. The field was expanded as a square, first with 2.3 and then 2.7 cm. The field was increased equally in the horizontal and vertical directions. When the field reached 35 cm x 35 cm the anti-scatter grid was removed and the exposures were repeated with the same field sizes.

### 3.1.4 Factor *R*

To evaluate the exposure with and without the anti-scatter grid, a factor $R$ was calculated as,

$$R = GF \cdot T_p \tag{3.1}$$

where grid factor $GF$ was the fraction between DAP with and without anti-scatter grid and $T_p$ was the transmission of primary radiation through the grid. $GF$ was calculated with DAP that was obtained after each exposure. $T_p$ was calculated as the fraction of measured radiation doses from exposures with and without the grid, to evaluate the amount of primary radiation reduced by the grid. The radiation dose was measured with a dosimeter RaySafe X2 (RaySafe) with a fixed mAs, with the grid perpendicular and at a distance 110 cm from the X-ray tube and the dosimeter 8 cm behind the centre of the grid. To limit the amount of scattered radiation, a narrow beam geometry was used during these measurements. A filter with 20 mm aluminium was used to represent a patient.

$R$ represents the change in AEC preset value to obtain an equal amount of primary radiation to the detector when removing the physical grid.

For each exposure of the three examined parameters, $R$ was calculated. Then the mean value of the five repeated exposures was computed and was presented with their standard deviation of the mean, to observe any variation in $R$.

## 3.2 Part 2: Scattered radiation from anthropomorphic phantoms

These measurements were performed at Mediel AB in Mölndal, with a radiography system (Arcoma Precision i5), on a detector with Built-in AEC Assistance (BiAA, Canon CXDI-420C) and a virtual anti-scatter grid called Scatter correction from Canon. An anti-scatter grid (JPI Healthcare), with a grid ratio of 10:1, a strip frequency of 52 lines/cm and a focal distance of 115 cm was used for examinations on a patient table. Another grid was used for a wall stand, with the same properties but with a focal distance of 180 cm. The BiAA detector had five AEC chambers, where each region had a width and a length of 7 cm, two chambers at the top and bottom and one chamber in the centre. More information about the detector can be found in Table A.11 in Appendix 1.

Each exposure was repeated five times consecutively with an anti-scatter grid, followed by five exposures without a grid, and the DAP, mAs, ms and EI were noted.

### 3.2.1 Phantoms

The measurements were executed on an adult upper body phantom (Kyoto Kagaku PBU-60), an adult pelvis phantom (OpenMedis SM01142) and a pediatric chest phantom (Kyoto Kagaku PBU-70). To increase the thickness of the adult upper body phantom, two different sizes of body plates were used. The two body plates

represented an adult of BMI 32 and 40 (Kyoto Kagaku). For the adult pelvis, PMMA was used to create a larger patient thickness and for the pediatric phantom, no increase in thickness was studied. The phantom thicknesses noted were measured at the thickest part of the phantom.

#### 3.2.1.1 Image technique: Adult chest

Examination of the adult chest began by choosing an examination protocol where the parameters manually were set to desirable values, after the phantom had been placed on the patient table. The exposure settings were set with the help of an application specialist. The adult chest was examined with both anteroposterior (AP) view, where the thickness was 21 cm, and lateral (LAT) view, with the thickest width of 29 cm. The AP view was examined with the tube voltages 125 and 141 kV and the field sizes 31 cm x 36.5 cm and 41.4 cm x 39.5 cm, the latter was to represent the field size set by a less precise radiographer. The LAT view was examined with 141 kV and the field sizes 30 cm x 25 cm and 38 x 41 cm on a wall stand. Before the chest examination the upper two AEC chambers were selected on the BiAA detector. These exposure settings were used repeatedly for the two different body plates and without the anti-scatter grid.

#### 3.2.1.2 Image technique: Adult pelvis

The adult pelvis phantom was placed on the patient table and a new examination protocol was selected with new exposure parameters. The pelvis phantom was examined in AP position but with two types of examinations, one examination of the whole pelvis and a second examination of the hip joint. The thicknesses of 23, 29, and 35 cm were evaluated in the two examination types. The whole pelvis examination had a fixed field size of 33.5 cm x 29.5 cm and tube current at 400 mA, but varied in tube voltage as 70 kV was applied for the thicknesses 23 and 29 cm but both 70 and 85 kV was used for 35 cm. As for the hip joint examination, the field sizes 15.8 cm x 19 cm and 17 cm x 22 cm were used. A tube voltage of 70 kV was set for 23 and 29 cm, and 90 kV for 35 cm.

The density was the same for all examination except the adult pelvis. The density was changed to -3 from 0, and other exposure settings were change to achieve the desirable dose to the AEC. This change needed to been done because the AEC back-up timer reached the limit.

#### 3.2.1.3 Image technique: Pediatric chest

The pediatric chest was placed on the patient table in AP position and started the examination with a tube current of 50 mA using a fixed tube voltage at 102 kV and a fixed field size of 25 cm x 18.2 cm. The exposure was then repeated with the tube current 25 mA. The top two AEC chambers were selected for the first measurement with 50 mA. The middle AEC chamber was chosen when the tube current changed to 25 mA.

### 3.2.2 Covering half of an AEC chamber

To evaluate the effects of patient misplacement over the AEC, a 7 cm thick phantom was placed over the center AEC chamber to represent small extremities. The field size was set to 7.5 cm x 6.7 cm to cover the whole chamber with the field. After one exposure over the whole AEC chamber, 1 mm of lead shield was placed over half of the AEC and the phantom covered the other half. Then, another exposure was done and the DAP, EI and mAs were recorded.

### 3.2.3 Calculated $R$

New factors $R$ were calculated from the DAP obtained from the examinations, and mean values of five repeated exposures were computed. The EI and mAs were also evaluated. The $R$ was then sorted by phantom, examination type, and thickness into three groups: small, medium, and large.

# 4

# Results

In this section, the results from the measurements are presented as the mean value of factor $R$, with their standard deviations ($\sigma$) of the mean value, out of five exposures with and five without an anti-scatter grid. DAP was used to calculate $R$ because the mAs did not give enough decimals for a precise evaluation. This applies to parts 1 and 2, if nothing else is mentioned. Each data point can be found in the Appendix. All the values of $R$ were calculated with a $T_p$ of 0.64, this value was obtained from the following exposures in Table 4.1 with a fixed mAs, and the dose was obtained by the dosimeter.

**Table 4.1:** $T_p$ for examinations with 70, 90 and 120 kV with fixed mAs.

| kV | mAs | radiation dose with grid [$\mu$Gy] | radiation dose with out grid [$\mu$Gy] | $T_p$ |
|---|---|---|---|---|
| 70 | 20 | 13.13 | 21.81 | 0.60 |
| 90 | 20 | 43.48 | 68.39 | 0.64 |
| 120 | 10 | 60.13 | 92.34 | 0.65 |

## 4.1 Part 1: Exposure with and without an anti-scatter grid on PMMA phantom

The removal of the anti-scatter grid resulted in a decreased DAP for all of the measurements. However, $R$ increased with increasing PMMA thickness, see Table 4.2. The greatest thickness, at 30 cm, also resulted in the highest $R$ of 3.74. The lowest $R$ of 2.32 was found at the thinnest PMMA, at 10 cm.

**Table 4.2:** Varying thickness of PMMA with 80 kV, 400 mA, and 20 cm x 20 cm in field size.

| Thickness [cm] | $R \pm \sigma$ |
|---|---|
| 10 | 2.32 ± 0.04 |
| 12 | 2.57 ± 0.12 |
| 15 | 2.75 ± 0.07 |
| 17 | 2.77 ± 0.05 |
| 20 | 3.00 ± 0.07 |
| 22 | 3.26 ± 0.06 |
| 25 | 3.35 ± 0.06 |
| 27 | 3.48 ± 0.06 |
| 30 | 3.74 ± 0.12 |

In general, increased kV showed a decreased $R$ for all the evaluated thicknesses. For 10 cm, the smallest $R$ of 1.23 was found at 130 kV and the largest of 2.58 at 60 kV, see Table 4.3, while the smallest and highest $R$ at 15 cm was found at 130 and 80 kV, with a value of 2.02 and 2.93 respectively. Table 4.3 also shows $R$ for 20 cm, the highest value of 3.27 was found at 70 kV. However, this mean value was calculated with only two data points. It was not possible to use 50 and 60 kV for the thicknesses 20, 25, and 30 cm, and 70 kV was not possible for 25 and 30 cm. The next highest $R$ was 3.19 found at 110 kV for 20 cm. The lowest $R$ was recorded at 130 kV, with a value of 2.91. Both the thicknesses 25 and 30 cm had the greatest $R$ at 80 kV of 3.50 and 3.92, but had different kV for their lowest recorded $R$ of 3.20 and 3.51 at 120 and 110 and 130 kV respectively.

**Table 4.3:** Varying kV for 10, 15, 20, 25 and 30 cm of PMMA, with 500 mA and 20 x 20 cm in field size.

| Tube voltage [kV] | $R \pm \sigma$ | | | | |
|---|---|---|---|---|---|
| | 10 cm | 15 cm | 20 cm | 25 cm | 30 cm |
| 50 | 2.40 ± 0.07 | 2.79* ± 0.12 | - | - | - |
| 60 | 2.58 ± 0.07 | 2.90* ± 0.07 | - | - | - |
| 70 | 2.34 ± 0.11 | 2.75 ± 0.07 | 3.27* ± 0.05 | - | - |
| 80 | 2.19 ± 0.06 | 2.93 ± 0.10 | 3.11 ± 0.09 | 3.50 ± 0.11 | 3.92 ± 0.29 |
| 90 | 1.84 ± 0.04 | 2.73 ± 0.03 | 3.10 ± 0.07 | 3.35 ± 0.12 | 3.67 ± 0.18 |
| 100 | 1.53 ± 0.09 | 2.61 ± 0.04 | 3.15 ± 0.09 | 3.32 ± 0.09 | 3.53 ± 0.21 |
| 110 | 1.45 ± 0.03 | 2.44 ± 0.08 | 3.19 ± 0.07 | 3.33 ± 0.11 | 3.51 ± 0.12 |
| 120 | 1.39 ± 0.06 | 2.34 ± 0.04 | 3.18 ± 0.13 | 3.20 ± 0.08 | 3.57 ± 0.15 |
| 130 | 1.23 ± 0.06 | 2.02 ± 0.05 | 2.91 ± 0.08 | 3.31 ± 0.06 | 3.51 ± 0.16 |

*This mean value was calculated with four data points, two with grid and two without grid.
-No data for this exposure setting.

The kV for both 10 and 15 cm, showed a clear decrease in $R$ with an increasing kV, see Figure 4.1. For the thicknesses 20, 25 and 30 cm, $R$ was more stable.

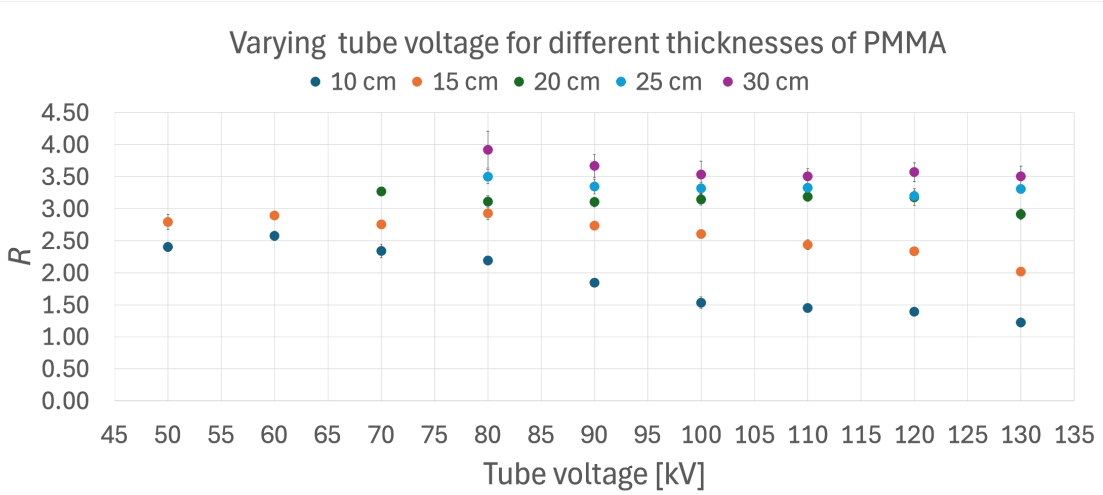


**Figure 4.1:** $R$ for the thicknesses 10, 15, 20, 25 and 30 cm of PMMA with varying kV, with 500 mA and a field size of 20 cm x 20 cm.

The increased field size resulted in an increased $R$, see Table 4.4. As field size increased from 15 cm x 15 cm to 17.3 cm x 17.3 cm, the $R$ increased by 10.5%, from 2.56 to 2.83. $R$ of 2.56 was the smallest determined $R$ in the variation of field sizes. The greatest difference was 11.3%, from the field size 17.3 cm x 17.3 cm to 20 cm x 20 cm. However, the greatest value of $R$ was 4.56 and was determined at the field size 35 cm x 35 cm.

**Table 4.4:** Varying field sizes for 20 cm of PMMA with 70 kV and 500 mA.

| Field size [cm x cm] | $R \pm \sigma$ |
|---|---|
| 15 x 15 | 2.56 ± 0.06 |
| 17.3 x 17.3 | 2.83 ± 0.12 |
| 20 x 20 | 3.15 ± 0.08 |
| 22.3 x 22.3 | 3.36 ± 0.08 |
| 25 x 25 | 3.68 ± 0.08 |
| 27.3 x 27.3 | 3.97 ± 0.12 |
| 30 x 30 | 4.16 ± 0.12 |
| 32.3 x 32.3 | 4.34 ± 0.09 |
| 35 x 35 | 4.56 ± 0.09 |

## 4.2 Part 2: Exposure on detectors with Built-in AEC Assistance

In the second part of this study, the BiAA detector was placed 115 cm from the X-ray tube and the phantoms were placed directly on the detector.

### 4.2.1 Adult chest phantom

The results from the adult chest AP examination showed an increased $R$ while both the thickness and field size increased respectively, see Table 4.5. $R$ was 1.13 at the thickness of 21 cm but increased to 1.36 for the thickness of 27 cm. For 32 cm, $R$ was 1.59, which is an increase of 17% from 1.36. For 125 kV and 32 cm in thickness, and an increased field size, from 31 cm x 36.5 cm to 38 cm x 41 cm, $R$ increased from 1.59 to 1.77. As the kV increased from 125 to 141 kV, for the field size 31 cm x 36.5 cm and 32 cm in thickness, $R$ resulted in a similar value, 1.59 and 1.58. More data is presented in Appendix 1.

**Table 4.5:** $R$ for AP examination with different settings of the adult chest phantom.

| kV | Field size [cm x cm] | Thickness [cm] | R $\pm$ $\sigma$ |
|---|---|---|---|
| 125 | 31 x 36.5 | 21 | 1.13 $\pm$ 0.03 |
| 125 | 31 x 36.5 | 27 | 1.36 $\pm$ 0.01 |
| 125 | 31 x 36.5 | 32 | 1.59 $\pm$ 0.05 |
| 125 | 38 x 41 | 32 | 1.77 $\pm$ 0.01 |
| 141 | 31 x 36.5 | 32 | 1.58 $\pm$ 0.01 |

The adult chest LAT examination, with 141 kV, resulted in $R$s of 1.20, 1.36 and 1.51 with the increased thicknesses of 29, 35, and 39 cm and field size of 30 cm x 25 cm. As the field increased from 30 cm x 25 cm to 38 x 41 cm, for the thickness of 39 cm and 141 kV, the $R$ increased from 1.51 to 1.56.

**Table 4.6:** $R$ for LAT examination with different settings of adult chest phantom, with 141 kV.

| Field Size [cm x cm] | Thickness [cm] | R $\pm$ $\sigma$ |
|---|---|---|
| 30 x 25 | 29 | 1.20 $\pm$ 0.06 |
| 30 x 25 | 35 | 1.36 $\pm$ 0.03 |
| 30 x 25 | 39 | 1.51 $\pm$ 0.04 |
| 38 x 41 | 39 | 1.56 $\pm$ 0.01 |

### 4.2.2 Adult pelvis phantom

The adult pelvis phantom was examined with two different examinations, the pelvis and the right hip joint. The pelvis resulted in an $R$ of 2.89, 3.49, and 4.13 for the thicknesses 23, 29, and 35 cm with 70 kV and field size 35.5 cm x 29.5 cm, see Table 4.7. Then 85 kV was used for 35 cm, this resulted in a decreased $R$, from 4.13 to 3.38, for the same field size. The same trend was observed for the hip examination, as the thickness increased from 23 to 29 cm with 70 kV, and the field size increased from 15.8 cm x 19 cm to 17 cm x 22.1 cm, $R$ increased from 2.34 to 2.95, see Table 4.8. Then 90 kV was used for 35 cm of thickness and an $R$ of 2.62 was calculated.

**Table 4.7:** $R$ for AP examination of adult pelvis phantom with field size 33.5 cm x 29.5 cm.

| kV | Thickness [cm] | $R \pm \sigma$ |
|---|---|---|
| 70 | 23 | 2.89 ±0.02 |
| 70 | 29 | 3.49 ±0.04 |
| 70 | 35 | 4.13 ± 0.12 |
| 85 | 35 | 3.38 ± 0.07 |

**Table 4.8:** $R$ for AP examination of the adult hip (pelvis phantom).

| kV | Field size [cm x cm] | Thickness [cm] | $R \pm \sigma$ |
|---|---|---|---|
| 70 | 15.8 x 19 | 23 | 2.34 ± 0.06 |
| 70 | 17 x 22.1 | 29 | 2.95 ±0.10 |
| 90 | 17 x 22.1 | 35 | 2.62 ±0.02 |

### 4.2.3 Pediatric chest phantom

The pediatric chest examination was performed with the upper left and right AEC chamber with 50 mA and the center AEC chamber with 25 mA, with the same field size of 25 cm x 18.2 cm. $R$ was calculated to 1.08 with 50 mA and 1.18 with 25 mA. The mAs received from the two different examinations were 0.40 and 0.31 with the grid and 0.25 and 0.18 without, see Appendix 1 Table A.16 and A.17.

### 4.2.4 Covering half of the AEC chamber

The DAP increased when half of the AEC center chamber was covered with 1 mm lead on the 7 cm thick phantom, using exposure settings of 60 kV and 7.1 cm x 6.3 cm in field size. The DAP was 1 mGycm$^2$ without any lead and then increased to 2 mGycm$^2$ when lead was placed on the half AEC chamber, for mAs and EI values see Table A.18 in Appendix 1.

### 4.2.5 Summarized table for the anthropomorphic phantom

Table 4.9 is a summarized table for all the adult anthropomorphic phantoms and their corresponding $R$s for the different examination thicknesses. The thicknesses were divided into three categories: small, medium, and large. The thinnest thickness examined for each phantom was placed into the category small, which means that the thickness is not the same but it is the thinnest for that type of phantom. The same categorization was applied to the categories medium and large. Not all the examined kV settings are presented in that table.

**Table 4.9:** Summarized table for the adult chest phantom and pelvis phantom and corresponding $R \pm \sigma$ for the thicknesses.

| Phantom | | Thickness | | |
|---|---|---|---|---|
| | | Small | Medium | Large |
| Chest AP | 125 kV | 1.13 ± 0.03 | 1.36 ± 0.01 | 1.59 ± 0.05 |
| Chest LAT | 141 kV | 1.20 ± 0.06 | 1.36 ± 0.03 | 1.51 ± 0.04 |
| Pelvis | 70 kV | 2.89 ± 0.02 | 3.49 ± 0.04 | 4.13 ± 0.12 |
| Hip | 70 kV | 2.34 ± 0.06 | 2.95 ± 0.10 | - |
| | 90 kV | - | - | 2.62 ± 0.02 |

# 5

# Discussion

This study aimed to find a factor $R$ for different parameter settings that can be used to adjust the AEC preset value, so that the amount of primary radiation to the detector remains constant when the grid is removed. By examining different kV, thicknesses and field sizes, when exposing PMMA phantoms, their contribution to the amount of scattered radiation was evaluated. Also, three anthropomorphic phantoms were examined with a BiAA detector, with and without an anti-scatter grid, and the scattered radiation was analyzed.

In the calculation of $R$, the reduction in the amount of primary radiation when using an anti-scatter grid was included with $T_p$, with a value of 0.64. This factor was chosen because of the low variation in $T_p$ for the different kV settings. To optimize $R$ further, $T_p$ should be recalculated when using different anti-scatter grids, because $T_p$ depends on the grid properties.

Examinations of the increasing PMMA thickness resulted in an increased $R$, see Table 4.2. These results were expected, since the amount of scattered radiation increases with increasing thickness, as stated in the theory section 2.1.3. The smallest $R$ of 2.32 was observed at 10 cm of PMMA and the largest $R$ of 3.74 at 30 cm. A similar increase in $R$ was observed when examining the three different anthropomorphic phantoms, although they were made of different materials. The increasing thickness resulted in an abrupt increase of $R$ for thinner PMMA compared to thicker thicknesses PMMA. The thicker PMMA, the more interactions occur and, therefore, the larger amount of scattered radiation was created. The general increase in $R$ due to the thickness indicates the importance of choosing an appropriate patient size adjustment in an examination protocol when no grid is used. The increase of scattered radiation results in an increased detector dose (Ahn et al., 2018).

An interesting finding was similar increase in $R$ with the increasing thicknesses of the adult chest and adult pelvis phantoms, around 40%, from the thinnest to the thickest phantom thickness, see Table 4.5 and 4.7. It can be argued that these anatomical regions had a larger impact on $R$ compared to the change in thickness. For example, the difference between adult chest AP for small and medium thickness was about 20.4 %, and for the same thicknesses for the pelvis, the difference was about 20.8%. The difference between chest and pelvis for the medium thickness was about 150 %.

$R$ represents the change in the AEC preset dose required to maintain the same amount of primary radiation reaching the detector when not using a grid, compared

to using AEC with a grid. The calculated $R$ is an estimate of how the exposure needs to vary with different patient thicknesses, rather than an absolute value. Nevertheless, the $R$ indicates the importance of proper thickness categorization when optimizing a gridless examination protocol. Therefore, if an improper patient size is selected during an examination, an over- or under exposure of the patient may occur, which in both cases is unfavorable.

Evaluation of $R$ presented an interesting result with the increasing kV along with an increasing PMMA thickness. It is evident that $R$ decreases with increasing kV for 10 and 15 cm of thickness, see Figure 4.1. For the thicknesses 20, 25, and 30 cm, $R$ was more stable, with small varieties, for different kV. One explanation to the less varying $R$s could be the decreasing probability for photoelectric effect with increasing kV, i.e. photon energy (Dance et al., 2014, chapter 2). The low-energy photons did not traverse these thicknesses and to the detector, independent of the kV. However, the opposite applies to 10 and 15 cm at low kV, where $R$ had a higher variation and the low-energy photons were registered by the detector because of the thinner PMMA. The variation of $R$, for the lower kV, can also be influenced by the kV dependence of the ionization chamber, but were not analyzed in this study.

The 50 and 60 kV could not be examined for the 20, 25 and 30 cm thick PMMA, because the back-up timer for the AEC was exceeded, and the exposure was not completed. A similar occurrence was observed for 70 kV, for the thicknesses of 25 and 30 cm. Hence, no $R$ was calculated. The 50 and 60 kV provided four data points for 15 cm of PMMA, this was caused by the back-up timer, but it occurred for three of the five repeated exposures. The back-up timer was increased before the exposures but could not be set too high due to the clinical relevance. It remains uncertain why the exposure was performed twice instead of not at all. The same happened for 70 kV for 20 cm thick PMMA, and $R$ was likewise calculated for two exposures.

The thicknesses between 10-20 cm of PMMA are more of a representative thickness for a pelvis or hip for children than adults, meanwhile it is the opposite for the thicknesses 20-30 cm. When increasing the kV from 80 to 90 kV, $R$ decreased for all thicknesses but in a higher extent for 10 cm. The increasing kV resulted in a less variation for $R$ between the thicknesses 20 to 30 cm, but still a decrease in $R$. The same trend was observed for the adult pelvis examination, as the kV increased it resulted in a decreased $R$. Table 4.7 shows this decrease, as the kV increased from 70 to 85 kV, for 35 cm of thickness, the $R$ decreased from 4.13 to 3.38. Since the thinner thicknesses of PMMA were more affected by the change in kV, these results must be taken in to account when considering using $R$ for examinations of children.

During the hip examination, the kV increased from 70 to 90 kV as the thickness increased from 29 to 35 cm, see Table 4.8. However, as discussed above, the increase in thickness increases $R$, but as the kV was increased along with the thickness, the $R$ was smaller for 35 cm with an $R$ of 2.62 compared to 2.95 for 29 cm. This result is noteworthy because it may imply that the impact on $R$ is more affected by the kV rather than the thickness. This can be explained by an increasing kV results in an increased average photon energy (Dance et al., 2014, chapter 6). A higher photon energy enables deeper penetration of the patient compared to lower energy photons.

The cross section for the photoelectric effect and Compton scatter also decreases with higher energies (Dance et al., 2014, chapter 6). However, the effect on $R$ may depend on the increase of kV in combination with the increase in thickness.

Theoretically, a higher kV gives a lower image contrast, which is why choosing an appropriate kV for a patient is important, depending on the tissues or structures inside the patient that is being examined. For example, adult chest examinations are performed around 120 kV and above (Sauter et al., 2019). The impact of the kV needs to be further investigated since the image quality was not evaluated in this study. The radiographer can have two options before a non-grid examination with BiAA, when including $R$, either decrease the scattered radiation with a higher kV or set a lower kV and increase the image contrast, depending on the type of examination. Since the virtual anti-scatter grid and additional software programs contribute to some reduction of image noise, one can argue for that a lower kV is preferable. Consequently, the AEC will receive more scattered radiation, but the virtual grid can reduce it. However, the balance between too high or enough radiation exposure is important and patient specific. For example, the patient thickness and anatomical region have to be considered. Unlike physical grids, virtual grids do not essentially reduce scatter, which may affect the signal-to-noise ratio. This study does not take this into consideration, but it is important to acknowledge that the grid effects the image quality in both contrast and noise characteristics.

The increasing field size increased $R$ when exposing the PMMA, see Table 4.4. The smallest $R$ of 2.56 was observed at the smallest field size examined, 15 cm x 15 cm. The largest $R$ of 4.56 was observed at the field size of 35 cm x 35 cm, which also was the largest field size examined on the 20 cm thick PMMA. $R$ increased in higher extent for the smaller field sizes than for the larger fields. This can be explained as a greater volume exposed will result in a larger amount of scattered radiation, because of more photon interactions, until a saturation level is reached (Dance et al., 2014, chapter 6). However, the scattered radiation should be limited, since the image quality would be reduced and, therefore, a suitable field size should be chosen for the examination type (Sayed et al., 2023). The same argument can be reasoned for $R$, to limit $R$ the field size should be kept small but still cover the anatomical region of interest.

The field sizes used in the study of the PMMA had a quadratic shape. Since patient examination does not always use quadratic shapes but instead more rectangle-shaped fields, with two distinct side lengths, these results of $R$ indicates an increasing scattered radiation with a larger field. A complete summary of how the general field shape for different examinations affects the scattered radiation is not evaluated in this study. However, the interaction probability is the same for every field size. $R$ increases with a larger field because the amount of scattered radiation will scatter towards the AEC more than for smaller fields, as less radiation scatter.

Different field sizes were used, compared with the PMMA examinations, when the anthropomorphic phantoms were examined. An overall larger field increases $R$. The adult chest AP examination was examined with two field sizes, 31 cm x 36.5 cm and 41.4 cm x 39.5 cm, for 32 cm of thickness and 125 kV, see Table 4.5. With the first field size mentioned, $R$ resulted in 1.59, and for the second field $R$ resulted in

1.77. These increases matches the increase of $R$ due to the field for the PMMA. Different field sizes were also used for the adult chest LAT examination, 30 cm x 25 cm and 38 cm x 41 cm, for the thickness 39 cm, see Table A.10. $R$ was 1.51 for the smaller field and 1.56 for the bigger one. Looking at the different field sizes, the AP examination had a smaller increase in area and a larger increase in $R$ compared to the LAT examination, even if there was a larger thickness examined for the LAT projection. However, the AP and LAT projections examined had different kV, the AP had 125 kV, and the LAT had 141 kV. This indicates that the kV may affect the scattered radiation more than the thickness and the field size since the resulting increase was smaller for the LAT projection.

Regardless of the differences in $R$ discussed above, the field size has an impact on the increasing amount of scatter radiation, if the thickness and kV are constant. The field size is an important exposure parameter that needs to be taken into account when a patient is examined. If a radiographer does not collimate the field enough and have a larger field than needed, it will result in an increase of the radiation dose to the patient.

The field size is an exposure parameter that can be difficult to involve with the application of $R$. The underlying factors in the uncertainties of the radiographer can be one cause, one cannot assume that every radiographer is precise enough or that everyone always collimates an exact field according to the anatomy in every examination. Even if the field size itself can be difficult to involve in the implementation of $R$ into the system, the interesting finding of the increasing $R$ with increasing field for different kV still needs to be considered in some way.

One limitation, regarding the field size, was the lack of PMMA to increase the field further than 35 cm x 35 cm. Some examinations, especially adult chest and pelvis examinations, require larger fields than 35 cm, which is why examinations with larger fields would have been beneficial for this study.

The pediatric phantom was examined with the center AEC and the upper left and right AEC. The $R$s for the different AEC chambers differed. The calculated $R$ for the upper left and right AEC was 1.08 and 1.18 for the center. There is a small increase in $R$ when the center AEC was selected and a possible explanation can be the change of anatomical structures in front of the AEC. The center chamber should be positioned behind the spinal cord of the phantom. By placing the phantom accordingly, the mAs have increased due to the larger amount of scattered radiation created by the higher density of the spinal cord, compared to the lungs. Using the measured mAs for exposure with and without the grid and the used mA, the exposure time can be calculated to 8 and 12 ms with the grid, and 5 and 7 ms without the grid, see Appendix 1 Table A.17. Exposure time is an important exposure parameter since it is one of the factors that controls the amount of radiation to the patient. In a radiography system, the exposure time cannot be too short, then the kV will not reach the set value and the generator needs some time to generate a stable AEC signal. One can argue that the exposure times for the gridless pediatric phantom examination are low, but this depends entirely on the manufacturer and model of the system used. Since children can unintentionally move during exposure, due to difficulties in following instructions, the low exposure times can be an advantage

to eliminate motion during exposure. An explanation of the low exposure times can potentially be that the pediatric phantom thickness/material may be too low in attenuation and does not contribute to a large amount of scattered radiation. $R$ was lower for the pediatric phantom than for the adult phantoms.

This study also evaluated examinations of small extremities, such as an arm or a wrist, with AEC and a gridless examination protocol. Using a small phantom on the BiAA detector and covering half of the center AEC with 1 mm lead, the system increased the exposure with a factor of two, as the DAP went from 1 to 2 mGycm$^2$. This may indicate that the AEC takes a mean value of all pixel values and then increases the exposure, since DAP increased. Due to only one conducted exposure with this set-up, and inadequate decimals for DAP, it makes it difficult to draw any conclusion.

The summarized table, Table 4.9, shows $R$ for the different anthropomorphic phantoms. Even though these phantoms had different thicknesses they were still divided into the thicknesses small, medium, and large. Between the thicknesses small and medium, $R$ increased about 20% for the AP adult chest examination. Between medium and large, the increase was similar, with about 17% for $R$. As for the pelvis examination, the increase in $R$ between small, medium, and large was similar to the chest examination, with 21% and 18%. These similar increases were interesting because the adult chest phantom and pelvis phantom are two very different phantoms but still have a similar increase between the the three thicknesses. However, $R$ for the pelvis phantom resulted in a higher $R$ for all thicknesses. This implies that the anatomical region examined is more important, for the AEC preset dose than choosing an exact matching thickness to the patient.

The foremost implementation of this study would be for bedside examinations with BiAA in the future. A gridless protocol in combination with AEC would ease the examinations for both the radiologists and the patients. This implementation would be a benefit because of the reduced risk of misaligning the grid to the X-ray tube. Anti-scatter grids can also be difficult to operate because of their weight. Even though this study is not complete, the $R$ calculated can be a guide for how to consider gridless exposures with AEC, since it was clear how the thickness, kV and field size matter individually. Research with more varying parameters would be beneficial in the future, in order to discuss the clinical application of examination with AEC without a grid.

$R$ can be implemented in a general radiographic system by optimizing the density steps. The density adjusts the exposure. By increasing or decreasing the density before an examination, the exposure will increase or decrease. These steps are set by the manufacturer but can be adjusted by the user. The density base, step 0, is set on a specific value, if the density changes, then the exposure would follow. The $R$s calculated could be implemented in the system by adjusting the increase or decrease in the density step. This may include a change to the density base. However, it should be studied more thoroughly.

Another implementation could be to involve $R$ in the selection of patient thickness. Before an examination, a patient size is selected that represents the same size of the patient being examined, small, medium, or large. As a thickness is set in the

examination protocol, the generator settings change, e.g. density and kV. $R$ could, in addition to the changes in density, as discussed above, adjust the kV further. $R$ may be included in other ways in the examination protocol, to optimize the correct use of the results in this study, further research is needed.

The antropomorphic phantom part of this study was compiled on the BiAA detector and not with a standard AEC system. However, the type of AEC should not affect the amount of radiation received which was measured. Something that could influence the obtained radiation is the positioning of the patient, as an increased distance to the AEC would decrease the amount of radiation (Dance et al., 2014, chapter 6). However, this could be studied further to see if different AEC systems affect the $R$.

This study sets the first steps for additional studies, but as with any study, there were limitations. The lack of evaluation of the obtained image and image quality was one limitation. The reason for this was the time constraint. To develop this study further, more anthropomorphic phantoms could be tested for different types of examination. Another limitation linked to the phantoms was how the adult pelvis phantom increased thickness compared to the adult upper body phantom. For the pelvis, PMMA was used to increase the thickness, which was not as optimal as the body plates for the upper body phantom. The body plates were a more representable thickness because the plates covered the phantom as real tissue, which the PMMA did not. The scattered radiation may exit these two phantoms differently since there was a gap between the PMMA and the side of the pelvis. The upper body phantom has a pelvis area, but there are gaps on both sides of the hips for that phantom. That was why the pelvis phantom with additional PMMA seemed to be a better option.

Additionally, the use of only one type of anti-scatter grid could affect the $R$. There are different grid ratios that will affect the primary and scattered radiation. Often, a specific grid is used for a specific type of examination to ensure sufficient primary radiation and reduced scattered radiation (Dance et al., 2014, chapter 6, Table 6.3). In this study, two grids were used for the anthropomorphic phantoms, one for the patient table and one for the wall stand. However, the grid ratio and the focal distance have a great impact on the amount of primary and scattered radiation that will reach the detector. This causes the limitations of implementing $R$ into different radiography systems and examination types. However, future studies would benefit from examinations with different types of grid ratios and other grid properties, such as line frequency.

Finally, the results of $R$ in this study were evaluated on PMMA and anthropomorphic phantoms, which are not exactly equal to the anatomy of a patient. $R$ can therefore differ for a real patient.

# 6

# Conclusion

This study aimed to find a factor $R$ for different parameter settings that can be used to adjust the AEC preset value, in order to maintain a constant amount of primary radiation to the detector when the anti-scatter grid is removed. $R$ varied with different parameters, e.g. when the phantom thickness and field size increased, $R$ also increased. When the kV increased, $R$ decreased. The adult chest phantom and pelvis phantom resulted in an equal relative increase of $R$ for different patient sizes. The results of $R$ in this study can act as a fundamental understanding, for first and foremost, application to bedside examinations with BiAA detectors.

The findings, that $R$ was affected by the three examined parameters, provide a primary basis that can, with further research, expand the usage of a gridless examination protocol with the AEC. To develop a greater understanding of examination with AEC without a grid, the image quality needs to be analyzed and an increased variation of exposure parameters and phantoms would be beneficial.

# Bibliography


Abela, N., Guilherme Couto, J., Zarb, F., & Mizzi, D. (2022). Evaluating the use of anti-scatter grids in adult knee radiography. *Radiography*, *28*(3), 663–667. https://doi.org/https://doi.org/10.1016/j.radi.2022.05.004

Ahn, S. Y., Chae, K. J., & Goo, J. M. (2018). The potential role of grid-like software in bedside chest radiography in improving image quality and dose reduction: An observer preference study. *Korean Journal of Radiology*, *19*(3), 526–533. https://doi.org/10.3348/kjr.2018.19.3.526

Almén, A. (2020). *2020:10 patientstråldoser vid röntgenundersökningar* [Accessed: 2024-12-12]. https://www.stralsakerhetsmyndigheten.se/publikationer/rapporter/stralskydd/2020/202010/

Cancerfonden. (2023). Röntgen - hur går det till och varför görs undersökningen? [Accessed: 2024-10-23]. https://www.cancerfonden.se/om-cancer/undersokningar/rontgen

Canon Inc. (2021). Canon's first clinical trial using medical imaging ai technology commences in japan [Accessed: 2024-11-12]. https://global.canon/en/news/2021/20210325-2.html

Canon Inc. (2023). Built-in AEC Assistance [Broschyr] [Accessed: 2024-11-15]. https://mce.canon/products/digital-radiography/cxdi-elite-series-flat-panel-detectors/img/BiAA_brochure_screen.pdf

Dance, D., Christofides, S., Maidment, A., McLean, I., & Ng, K. (Eds.). (2014). *Diagnostic radiology physics*. INTERNATIONAL ATOMIC ENERGY AGENCY. https://www.iaea.org/publications/8841/diagnostic-radiology-physics

Fritz, S., & Jones, A. K. (2014). Guidelines for anti-scatter grid use in pediatric digital radiography. *Pediatric Radiology*, *44*, 313–321. https://doi.org/10.1007/s00247-013-2824-9

Ghafarian, P., Ay, M., Ghadiri, H., Sarkar, S., & Zaidi, H. (2007). Impact of x-ray tube voltage, field size and object thickness on scattered radiation distribution in diagnostic radiology: A monte carlo investigation. *2007 IEEE Nuclear Science Symposium Conference Record*, *5*, 3830–3834. https://doi.org/10.1109/NSSMIC.2007.4436956

Gibson, D. J., & Davidson, R. A. (2012). Exposure creep in computed radiography: A longitudinal study. *Academic Radiology*, *19*(4), 458–462. https://doi.org/https://doi.org/10.1016/j.acra.2011.12.003

IAEA. (2024). Automatic exposure control devices [Accessed: 2024-11-19]. https://humanhealth.iaea.org/HHW/MedicalPhysics/DiagnosticRadiology/PerformanceTesting/Automaticexposurecontroldevices/index.html

Lança, L., & Silva, A. (2009). Digital radiography detectors – a technical overview: Part 1. *Radiography*, *15*(1), 58–62. https://www.sciencedirect.com/science/article/pii/S1078817408000102

Mekis, N., Bianchi, T., Doyle, C., Gauchat, M., Geerling, I., Linneman, J., Staats, S., & Campeanu, C. (2024). Gridless adult cervical spine radiography and its' effect on image quality and radiation dose: A phantom study. *Radiography*, *30*(1), 359–366. https://doi.org/https://doi.org/10.1016/j.radi.2023.12.009

Philips. (2015). Skyflow plus: Scatter correction for non-grid x-ray exams [Accessed: 2024-11-20]. https://www.philips.se/healthcare/resources/landing/sky-flow-plus#u59contactwidget=sales

Precht, H., Mørup, S., Tingberg, A., Outzen, C., Kusk, K., Nielsen, R., Midtgård, M., Winther, M., Waaler, D., & Kusk, M. (2019). Can scatter correction software replace a grid in dr pelvic examinations? *Radiation Protection Dosimetry*, *187*(1), 8–16. https://doi.org/10.1093/rpd/ncz129

Rosa, I. V., Furlan, L. N., Lykawka, R., Anés, M., Bacelar, A., & Dias, J. H. (2024). Analysis of exposure indices from digital radiography exams. *Brazilian Journal of Radiation Sciences*, 1–12. https://www.bjrs.org.br/revista/index.php/REVISTA/article/view/2435/1485

Šabič, I. (2016). The effect of anti-scatter grid on radiation dose in chest radiography in children. *Paediatrics Today*, *12*, 75–80. https://doi.org/10.5457/p2005-114.138

Sanna Axelsson. (2023). *Lungor – liggande*. Version 5.0. Radiologisk mottagning Norra Älvsborgs Länssjukhus, Radiologisk mottagning Uddevalla Sjukhus. https://mellanarkiv-offentlig.vgregion.se/alfresco/s/archive/stream/public/v1/source/available/sofia/nu10095-1819752655-373/surrogate

Sauter, A. P., Andrejewski, J., De Marco, F., et al. (2019). Optimization of tube voltage in x-ray dark-field chest radiography. *Scientific Reports*, *9*, 8699. https://doi.org/10.1038/s41598-019-45256-2

Sayed, M., Knapp, K. M., Fulford, J., Heales, C., & Alqahtani, S. J. (2023). The principles and effectiveness of x-ray scatter correction software for diagnostic x-ray imaging: A scoping review. *European Journal of Radiology*, *158*, 110600. https://doi.org/https://doi.org/10.1016/j.ejrad.2022.110600

Seibert, J. A., & Morin, R. L. (2011). The standardized exposure index for digital radiography: An opportunity for optimization of radiation dose to

the pediatric population. *Pediatric Radiology*, *41*(5), 573–581. https://doi.org/10.1007/s00247-010-1954-6

Strålsäkerhetsmyndigheten. (2017). Berättigande och optimering inom sjuk- och tandvård [Last updated: 01 September 2017. Accessed: 2024-12-11]. https://www.stralsakerhetsmyndigheten.se/omraden/sjuk--och-tandvard/berattigande-och-optimering/

Strålsäkerhetsmyndigheten. (2024). Ordlista kärnkraft: A-j [Accessed: 2024-11-12]. https://www.stralsakerhetsmyndigheten.se/omraden/karnkraft/ordlista-karnkraft/a-j/

Sy, E., Samboju, V., & Mukhdomi, T. (2024). X-ray image production procedures [Updated: 2022-10-17]. In *Statpearls [internet]*. StatPearls Publishing. https://www.ncbi.nlm.nih.gov/books/NBK564352/

Verstreepen, L., Wanninger, F., Apgar, B., & B.Hoberg. (2023). *Non-grid bedside chest imaging*. https://www.agfa.com/he/global/en/internet/he/library/libraryopen?ID=57395131

# A

# Appendix 1

Appendix 1 shows values over examination data from examination of PMMA and the three anthropomorphic phantoms, as well as data from covering half of an AEC chamber.

**Table A.1:** DAP with and without grid for various thicknesses and with exposure settings of 80 kVp, 400 mA and 20 cm x 20 cm in field size.

| Thickness [cm] | DAP w/ grid [mGycm$^2$] | DAP w/o grid [mGycm$^2$] |
|---|---|---|
| 10 | 14 | 4 |
| | 14 | 4 |
| | 15 | 4 |
| | 15 | 4 |
| | 15 | 4 |
| 12 | 22 | 5 |
| | 23 | 6 |
| | 23 | 6 |
| | 22 | 5 |
| | 23 | 6 |
| 15 | 42 | 9 |
| | 43 | 10 |
| | 44 | 10 |
| | 40 | 10 |
| | 43 | 10 |
| 17 | 69 | 15 |
| | 66 | 15 |
| | 67 | 16 |
| | 66 | 15 |
| | 67 | 16 |
| 20 | 123 | 26 |
| | 129 | 26 |
| | 116 | 27 |
| | 131 | 27 |
| | 128 | 27 |

*Continued on next page*

*Continued on next page*

| Thickness [cm] | DAP w/ grid [mGycm$^2$] | DAP w/o grid [mGycm$^2$] |
|---|---|---|
| 22 | 182 | 37 |
| | 190 | 37 |
| | 199 | 37 |
| | 190 | 39 |
| | 199 | 37 |
| 25 | 336 | 68 |
| | 356 | 66 |
| | 363 | 67 |
| | 370 | 70 |
| | 361 | 68 |
| 27 | 522 | 98 |
| | 528 | 97 |
| | 527 | 97 |
| | 562 | 101 |
| | 552 | 99 |
| 30 | 973 | 164 |
| | 1036 | 172 |
| | 969 | 174 |
| | 1080 | 181 |
| | 1086 | 184 |

*End of table.*

**Table A.2:** DAP and mAs with and without grid for various kV on 10 cm of PMMA, with the exposure settings 500 mA and 20 cm x 20 cm in field size.

| kV | DAP w/ grid [mGycm$^2$] | mAs w/ grid | DAP w/o grid [mGycm$^2$] | mAs w/o grid |
|---|---|---|---|---|
| 50 | 51 | 29 | 13 | 8.5 |
| | 52 | 29.5 | 13 | 8.5 |
| | 51 | 29 | 14 | 8.5 |
| | 51 | 29 | 13 | 8.5 |
| | 52 | 29 | 15 | 8.5 |
| 60 | 31 | 9.5 | 8 | 3 |
| | 32 | 10 | 7 | 3 |
| | 33 | 10 | 8 | 3 |
| | 31 | 10 | 8 | 3 |
| | 31 | 10 | 8 | 3 |
| 70 | 21 | 4.5 | 5 | 1.5 |
| | 20 | 4.5 | 6 | 1.5 |
| | 20 | 4.5 | 6 | 1.5 |
| | 21 | 4.5 | 5 | 1.5 |

*Continued on next page*

*Continued on next page*

| kV | DAP w/ grid [mGycm$^2$] | mAs w/ grid | DAP w/o grid [mGycm$^2$] | mAs w/o grid |
|---|---|---|---|---|
| | 21 | 4.5 | 6 | 1.5 |
| 80 | 14 | 2.5 | 4 | 1.0 |
| | 13 | 2.5 | 4 | 1.0 |
| | 15 | 2.5 | 4 | 1.0 |
| | 13 | 2.5 | 4 | 1.0 |
| | 14 | 2.5 | 4 | 1.0 |
| 90 | 11 | 1.5 | 4 | 1.0 |
| | 11 | 1.5 | 4 | 1.0 |
| | 12 | 2 | 4 | 1.0 |
| | 12 | 1.5 | 4 | 1.0 |
| | 12 | 1.5 | 4 | 1.0 |
| 100 | 10 | 1.5 | 5 | 1.0 |
| | 11 | 1.5 | 4 | 1.0 |
| | 10 | 1.5 | 4 | 1.0 |
| | 11 | 1.5 | 5 | 1.0 |
| | 11 | 1.5 | 4 | 1.0 |
| 110 | 11 | 1.5 | 5 | 1.0 |
| | 11 | 1.5 | 5 | 1.0 |
| | 12 | 1.5 | 5 | 1.0 |
| | 12 | 1.5 | 5 | 1.0 |
| | 11 | 1.5 | 5 | 1.0 |
| 120 | 11 | 1.0 | 5 | 1.0 |
| | 11 | 1.5 | 5 | 1 |
| | 12 | 1.0 | 6 | 1.0 |
| | 12 | 1.0 | 5 | 1.0 |
| | 11 | 1.0 | 5 | 1.0 |
| 130 | 10 | 1.0 | 5 | 1.0 |
| | 11 | 1.0 | 6 | 1.0 |
| | 11 | 1.0 | 5 | 1.0 |
| | 11 | 1.0 | 6 | 1.0 |
| | 11 | 1.0 | 6 | 1.0 |

**Table A.2:** Varying kV for 10 cm of PMMA.

*End of table.*

**Table A.3:** DAP and mAs with and without grid for various kV on 15 cm of PMMA, with the exposure settings 500 mA and 20 cm x 20 cm in field size.

| kV | DAP w/ grid [mGycm$^2$] | DAP w/o grid [mGycm$^2$] | mAs w/ grid | mAs w/o grid |
|---|---|---|---|---|
| 50 | 186 | 105 | 40 | 23.5 |

*Continued on next page*

*Continued on next page*

| kV | DAP w/ grid [mGycm$^2$] | DAP w/o grid [mGycm$^2$] | mAs w/ grid | mAs w/o grid |
|---|---|---|---|---|
| | 174 | 98 | 42 | 24 |
| 60 | 103 | 31.5 | 22 | 7.5 |
| | 102 | 31 | 23 | 7.5 |
| 70 | 64 | 13 | 15 | 3.5 |
| | 62 | 12.5 | 15 | 3.5 |
| | 67 | 13.5 | 14 | 3.5 |
| | 66 | 13 | 15 | 3.5 |
| | 66 | 13.5 | 16 | .5 |
| 80 | 41 | 6.5 | 2.5 | 1.0 |
| | 43 | 6.5 | 2.5 | 1.0 |
| | 45 | 7 | 2.5 | 1.0 |
| | 46 | 6.5 | 2.5 | 1.0 |
| | 46 | 7 | 2.5 | 1.0 |
| 90 | 34 | 4 | 1.5 | 1.0 |
| | 33 | 4 | 1.5 | 1.0 |
| | 35 | 4 | 2 | 1.0 |
| | 35 | 4.5 | 1.5 | 1.0 |
| | 35 | 4.5 | 1.5 | 1.0 |
| 100 | 32 | 3.5 | 8 | 1 |
| | 34 | 3.5 | 8 | 1 |
| | 32 | 3.5 | 8 | 1 |
| | 32 | 3.5 | 8 | 1 |
| | 34 | 3.5 | 8 | 1.5 |
| 110 | 33 | 3 | 8 | 1 |
| | 31 | 3 | 9 | 1 |
| | 33 | 3 | 9 | 1 |
| | 32 | 3 | 8 | 1 |
| | 32 | 3 | 8 | 1 |
| 120 | 29 | 2.5 | 8 | 1 |
| | 29 | 2.5 | 8 | 1 |
| | 28 | 2 | 8 | 1 |
| | 31 | 2.5 | 8 | 1 |
| | 30 | 2.5 | 8 | 1 |
| 130 | 25 | 2 | 8 | 1 |
| | 25 | 2 | 8 | 1 |
| | 24 | 2 | 8 | 1 |
| | 25 | 2 | 8 | 1 |
| | 28 | 2 | 8 | 1 |

**Table A.3:** Varying kV for 15 cm of PMMA.

*End of table.*

**Table A.4:** DAP and mAs with and without grid for various kV on 20 cm of PMMA, with the exposure settings 500 mA and 20 cm x 20 cm in field size.

| kV | DAP w/ grid [mGycm$^2$] | mAs w/ grid | DAP w/o grid [mGycm$^2$] | mAs w/o grid |
|---|---|---|---|---|
| 70 | 196 | 38.5 | 38 | 8 |
| | 200 | 39 | 39 | 8 |
| 80 | 127 | 18 | 27 | 4.5 |
| | 130 | 18.5 | 25 | 4 |
| | 130 | 18.5 | 29 | 4.5 |
| | 138 | 19.5 | 26 | 4 |
| | 131 | 18.5 | 27 | 4.5 |
| 90 | 102 | 11.5 | 19 | 2.5 |
| | 95 | 10.5 | 21 | 3 |
| | 102 | 11 | 21 | 3 |
| | 102 | 11.5 | 21 | 3 |
| | 102 | 11.5 | 21 | 3 |
| 100 | 93 | 8.5 | 18 | 2 |
| | 89 | 8 | 18 | 2 |
| | 94 | 8.5 | 20 | 2 |
| | 96 | 8.5 | 19 | 2 |
| | 98 | 9 | 20 | 2.5 |
| 110 | 90 | 7 | 18 | 2 |
| | 86 | 6.5 | 18 | 2 |
| | 97 | 7.5 | 18 | 2 |
| | 92 | 7 | 19 | 2 |
| | 91 | 7 | 18 | 2 |
| 120 | 74 | 5 | 17 | 1.5 |
| | 80 | 5.5 | 16 | 1.5 |
| | 86 | 5.5 | 18 | 1.5 |
| | 84 | 5.5 | 15 | 1.5 |
| | 86 | 5.5 | 16 | 1.5 |
| 130 | 73 | 4.5 | 15 | 1.5 |
| | 68 | 4 | 17 | 1.5 |
| | 75 | 4.5 | 16 | 1.5 |
| | 74 | 4.5 | 15 | 1.5 |
| | 72 | 4.5 | 16 | 1.5 |

**Table A.4:** Varying kV for 20 cm of PMMA.
*End of table.*

**Table A.5:** DAP and mAs with and without grid for various kV on 25 cm of PMMA, with the exposure settings 500 mA and 20 cm x 20 cm in field size.

| kV | DAP w/ grid [mGycm$^2$] | DAP w/o grid [mGycm$^2$] | mAs w/ grid | mAs w/o grid |
|---|---|---|---|---|
| 80 | 401 | 55 | 71 | 10.5 |
| | 379 | 52 | 66 | 9.5 |
| | 393 | 54 | 73 | 10.5 |
| | 376 | 52 | 71 | 10 |
| | 389 | 53.5 | 71 | 10.5 |
| 90 | 305 | 32.5 | 52 | 6 |
| | 285 | 30.5 | 57 | 6.5 |
| | 289 | 30.5 | 55 | 6.5 |
| | 279 | 29.5 | 54 | 6 |
| | 285 | 30 | 56 | 6.5 |
| 100 | 270 | 23 | 50 | 5 |
| | 269 | 23 | 49 | 4.5 |
| | 247 | 21.5 | 50 | 4.5 |
| | 255 | 22 | 50 | 5 |
| | 254 | 22 | 49 | 4.5 |
| 110 | 253 | 18 | 48 | 4 |
| | 238 | 17 | 46 | 4 |
| | 233 | 17 | 46 | 4 |
| | 252 | 18 | 48 | 4 |
| | 244 | 17.5 | 45 | 3.5 |
| 120 | 206 | 13 | 43 | 3 |
| | 209 | 13 | 41 | 3 |
| | 208 | 13 | 43 | 3 |
| | 212 | 13 | 40 | 3 |
| | 216 | 13.5 | 42 | 3 |
| 130 | 194 | 10.5 | 38 | 2.5 |
| | 191 | 10.5 | 38 | 2.5 |
| | 196 | 10.5 | 37 | 2.5 |
| | 198 | 10.5 | 38 | 2.5 |
| | 194 | 10.5 | 36 | 2.5 |

**Table A.5:** Varying kV for 25 cm of PMMA.
*End of table.*

**Table A.6:** DAP and mAs with and without grid for various kV on 30 cm of PMMA, with the exposure settings 500 mA and 20 cm x 20 cm in field size.

| kV | DAP w/ grid [mGycm$^2$] | DAP w/o grid [mGycm$^2$] | mAs w/ grid | mAs w/o grid |
|---|---|---|---|---|
| 80 | 1007 | 139 | 162 | 23 |
| | 1004 | 138.5 | 167 | 23.5 |
| | 1191 | 163.5 | 186 | 26 |
| | 1129 | 155.5 | 188 | 26.5 |
| | 1144 | 157.5 | 185 | 26 |
| 90 | 754 | 80 | 127 | 14 |
| | 718 | 76 | 125 | 13.5 |
| | 805 | 85 | 143 | 15.5 |
| | 785 | 83 | 136 | 15 |
| | 769 | 81.5 | 133 | 14.5 |
| 100 | 620 | 53 | 115 | 10.5 |
| | 642 | 55 | 108 | 9.5 |
| | 699 | 59.5 | 128 | 11.5 |
| | 690 | 59 | 122 | 11 |
| | 668 | 57 | 124 | 11 |
| 110 | 595 | 42.5 | 111 | 8.5 |
| | 593 | 42.5 | 108 | 8 |
| | 632 | 45 | 113 | 8.5 |
| | 626 | 44.5 | 112 | 8.5 |
| | 647 | 46 | 117 | 10.5 |
| 120 | 508 | 31 | 93 | 6 |
| | 518 | 31.5 | 96 | 6.5 |
| | 560 | 34 | 97 | 6.5 |
| | 536 | 32.5 | 100 | 6.5 |
| | 574 | 35 | 94 | 6 |
| 130 | 455 | 24 | 80 | 4.5 |
| | 449 | 24 | 82 | 4.5 |
| | 478 | 25.5 | 86 | 5 |
| | 468 | 25 | 89 | 5 |
| | 499 | 26.5 | 89 | 5 |

**Table A.6:** Varying kV for 30 cm of PMMA.
*End of table.*

**Table A.7:** AP examination of the adult chest phantom with 80 mA.

| kV | Thickness [cm] | DAP w/ grid [mGycm$^2$] | DAP w/o grid [mGycm$^2$] | mAs w/ grid | mAs w/o grid | EI w/ grid | EI w/o grid |
|---|---|---|---|---|---|---|---|
| 125 | 21 | 44 | 24 | 0.8 | 0.48 | 187 | 337 |
| | | 45 | 25 | 0.8 | 0.48 | 187 | 347 |
| | | 44 | 25 | 0.8 | 0.48 | 185 | 345 |
| | | 46 | 28 | 0.8 | 0.48 | 188 | 390 |
| | | 47 | 25 | 0.88 | 0.48 | 197 | 343 |
| | 27 | 83 | 38 | 1.44 | 0.72 | 181 | 332 |
| | | 84 | 40 | 1.44 | 0.72 | 182 | 335 |
| | | 83 | 39 | 1.44 | 0.72 | 181 | 334 |
| | | 83 | 39 | 1.44 | 0.72 | 180 | 328 |
| | | 83 | 39 | 1.44 | 0.72 | 179 | 332 |
| | 32 | 201 | 90 | 3.52 | 1.6 | 207 | 410 |
| | | 202 | 79 | 3.6 | 1.36 | 209 | 354 |
| | | 203 | 78 | 3.52 | 1.36 | 208 | 351 |
| | | 203 | 79 | 3.52 | 1.36 | 210 | 353 |
| | | 204 | 78 | 3.44 | 1.36 | 209 | 354 |
| 125 | 32<br>41.4 cm x 39.5 cm | 297 | 106 | 3.52 | 1.28 | 216 | 358 |
| | | 298 | 108 | 3.52 | 1.28 | 218 | 360 |
| | | 297 | 107 | 3.52 | 1.28 | 219 | 363 |
| | | 298 | 107 | 3.6 | 1.28 | 219 | 360 |
| | | 300 | 107 | 3.52 | 1.28 | 218 | 358 |
| 141 | 32<br>30.9 cm x 36.5 cm | 193 | 79 | 2.72 | 1.12 | 243 | 401 |
| | | 196 | 79 | 2.72 | 1.12 | 242 | 401 |
| | | 196 | 79 | 2.72 | 1.04 | 245 | 395 |
| | | 196 | 79 | 2.64 | 1.04 | 243 | 396 |
| | | 198 | 78 | 2.72 | 1.12 | 247 | 398 |

**Table A.8:** AP examination of the adult chest phantom, with 25 mA, 125 kV and 141 kV

| Thickness [cm] | ms w/ grid | ms w/o grid |
|---|---|---|
| 21 | 10 | 6 |
| | 10 | 6 |
| | 10 | 6 |
| | 10 | 6 |
| | 11 | 6 |
| 27 | 18 | 9 |
| | 18 | 9 |
| | 18 | 9 |
| | 18 | 9 |
| | 18 | 9 |
| 32 | 44 | 20 |
| | 45 | 17 |
| | 44 | 17 |
| | 44 | 17 |
| | 43 | 17 |
| 32 (41.4 cm x 39.5 cm) | 44 | 16 |
| | 44 | 16 |
| | 44 | 16 |
| | 45 | 16 |
| | 44 | 16 |
| 32 (141 kV) | 34 | 14 |
| | 34 | 14 |
| | 34 | 14 |
| | 33 | 13 |
| | 34 | 13 |

**Table A.9:** LAT examination of the adult chest phantom with 25 mA and 141 kV.

| Thickness [cm] | DAP w/ grid [mGycm$^2$] | DAP w/o grid [mGycm$^2$] | mAs w/ grid | mAs w/o grid | EI w/ grid | EI w/o grid |
|---|---|---|---|---|---|---|
| 29 | 10 | 5 | 0,625 | 0.325 | 50 | 60 |
| | 11 | 6 | 0.675 | 0.325 | 47 | 60 |
| | 10 | 5 | 0.65 | 0.325 | 46 | 61 |
| | 11 | 6 | 0.675 | 0.325 | 46 | 59 |
| | 11 | 6 | 0.65 | 0.325 | 47 | 58 |
| 35 | 22 | 11 | 1.4 | 0.65 | 38 | 46 |
| | 22 | 10 | 1.4 | 0.6 | 37 | 44 |
| | 22 | 11 | 1.6 | 0.7 | 40 | 45 |
| | 23 | 10 | 1.55 | 0.625 | 37 | 43 |
| | 22 | 10 | 1.6 | 0.6 | 36 | 43 |
| 39 | 36 | 15 | 2.3 | 1 | 64 | 45 |
| | 36 | 16 | 2.325 | 1.025 | 56 | 45 |
| | 38 | 14 | 2.325 | 0.95 | 57 | 51 |
| | 36 | 16 | 2.575 | 0.975 | 65 | 47 |
| | 37 | 16 | 2.325 | 1.025 | 66 | 45 |
| 39 (38 cm x 40.8 cm) | 71 | 29 | 2.2 | 0.925 | 50 | 55 |
| | 71 | 28 | 2.525 | 0.925 | 51 | 57 |
| | 70 | 29 | 2.225 | 0.925 | 50 | 58 |
| | 72 | 29 | 2.2 | 0.875 | 50 | 58 |
| | 70 | 29 | 2.2 | 0.875 | 49 | 57 |

**Table A.10:** LAT examination of the adult chest phantom, with 80 mA and 141 kV.

| Thickness [cm] | ms w/ grid | ms w/o grid |
|---|---|---|
| 29 | 25 | 13 |
| | 27 | 13 |
| | 26 | 13 |
| | 27 | 13 |
| | 26 | 13 |
| 35 | 56 | 26 |
| | 56 | 24 |
| | 64 | 28 |
| | 62 | 25 |
| | 64 | 24 |
| 39 | 92 | 40 |
| | 93 | 41 |
| | 93 | 38 |
| | 103 | 39 |
| | 93 | 41 |
| 39 (38 cm x 40.8 cm) | 88 | 37 |
| | 101 | 37 |
| | 89 | 37 |
| | 88 | 35 |
| | 88 | 35 |

**Table A.11:** Information about the digital detector CXDI-420C Wireless

| Thickness | Width | Length | Effective image area | Image matrix | Scintillator material |
|---|---|---|---|---|---|
| 15.7 mm | 460 mm | 460 mm | 430 x 430 mm | 3408 x 3408 pixels | Cesium Iodide (CsI) |

**Table A.12:** Examination of adult pelvis phantom, with sensitivity +1 and density -3. A field size of 33.5 cm x 29.5 cm, 400 mA and 70 and 85 kV was used.

| Thickness | DAP w/ grid [mGycm$^2$] | DAP w/o grid [mGycm$^2$] | mAs w/ grid | mAs w/o grid | EI w/ grid | EI w/o grid |
|---|---|---|---|---|---|---|
| 23 | 639 | 140 | 44.8 | 10.4 | 186 | 203 |
| | 640 | 141 | 45.2 | 10.4 | 189 | 206 |
| | 644 | 141 | 45.2 | 10.4 | 189 | 206 |
| | 643 | 141 | 45.2 | 10.4 | 190 | 206 |
| | 642 | 142 | 45.2 | 10.4 | 189 | 206 |
| 29 | 567 | 103 | 39.6 | 7.6 | 48 | 52 |
| | 577 | 104 | 40.8 | 7.6 | 49 | 51 |

*Continued on next page*

*Continued on next page*

| Thickness | DAP w/ grid [mGycm$^2$] | DAP w/o grid [mGycm$^2$] | mAs w/ grid | mAs w/o grid | EI w/ grid | EI w/o grid |
|---|---|---|---|---|---|---|
| | 572 | 103 | 40 | 7.6 | 50 | 51 |
| | 569 | 105 | 39.6 | 7.6 | 49 | 52 |
| | 565 | 104 | 39.2 | 7.6 | 48 | 52 |
| 35 | 1838 | 280 | 126.8 | 19.6 | 47 | 50 |
| | 1869 | 290 | 19.6 | 20.8 | 47 | 50 |
| | 1831 | 279 | 20.8 | 19.6 | 47 | 49 |
| | 1780 | 286 | 19.6 | 20.4 | 45 | 50 |
| | 1895 | 282 | 20.4 | 20 | 49 | 50 |
| 35 (85 kV) | 816 | 160 | 35.2 | 7.2 | 47 | 53 |
| | 824 | 156 | 35.6 | 7.2 | 48 | 52 |
| | 843 | 157 | 37.2 | 7.2 | 50 | 51 |
| | 852 | 157 | 36.4 | 7.2 | 50 | 52 |
| | 845 | 156 | 37.2 | 7.2 | 50 | 51 |

*End of table.*

**Table A.13:** Examination of adult pelvis phantom (ms values), when 400 mA, 70 and 85 kV was used.

| Thickness | ms w/ grid | ms w/o grid |
|---|---|---|
| 29 | 112 | 26 |
| | 113 | 26 |
| | 113 | 26 |
| | 113 | 26 |
| | 113 | 26 |
| 35 | 99 | 19 |
| | 102 | 19 |
| | 100 | 19 |
| | 99 | 19 |
| | 98 | 19 |
| 39 | 317 | 49 |
| | 321 | 52 |
| | 314 | 49 |
| | 306 | 51 |
| | 326 | 50 |
| 39 | 88 | 18 |
| | 89 | 18 |
| | 93 | 18 |
| | 91 | 18 |
| | 93 | 18 |

*End of table.*

**Table A.14:** Examination of hip (pelvis phantom).

| Thickness [cm] | Field size [cm x cm] | kV | DAP w/ grid [mGycm$^2$] | DAP w/o grid [mGycm$^2$] | mAs w/ grid | mAs w/o grid |
|---|---|---|---|---|---|---|
| 23 | 15.8 x 19 | 70 | 194 | 50 | 35 | 9.4 |
| | | | 185 | 52 | 33 | 9.4 |
| | | | 190 | 52 | 33.8 | 9.4 |
| | | | 188 | 51 | 33.5 | 9.4 |
| | | | 190 | 52 | 33.7 | 9.4 |
| 29 | 17 x 22 | 70 | 689 | 149 | 125 | 27.5 |
| | | | 707 | 149 | 128.5 | 27.5 |
| | | | 714 | 159 | 130.5 | 29.5 |
| | | | 701 | 152 | 127.5 | 28 |
| | | | 704 | 148 | 128 | 28 |
| 35 | 17 x 22 | 90 | 1046 | 255 | 105.5 | 26 |
| | | | 1059 | 254 | 106 | 26 |
| | | | 1052 | 256 | 105 | 26 |
| | | | 1060 | 254 | 106 | 26 |
| | | | 1039 | 256 | 104 | 26 |

**Table A.15:** Examination of adult pelvis phantom (ms values) with 70 and 90 kV.

| Thickness [cm] | EI w/ grid | EI w/o grid | ms w/ grid | ms w/o grid |
|---|---|---|---|---|
| 23 | 198 | 169 | 0.35 | 0.094 |
| | 188 | 169 | 0.33 | 0.094 |
| | 192 | 169 | 0.338 | 0.094 |
| | 191 | 169 | 0.335 | 0.094 |
| | 190 | 169 | 0.337 | 0.094 |
| 29 | 180 | 152 | 0.25 | 0.055 |
| | 185 | 153 | 0.257 | 0.055 |
| | 187 | 164 | 0.261 | 0.059 |
| | 182 | 157 | 0.255 | 0.056 |
| | 184 | 152 | 0.256 | 0.056 |
| 35 | 186 | 166 | 0.211 | 0.052 |
| | 188 | 165 | 0.212 | 0.052 |
| | 187 | 169 | 0.21 | 0.052 |
| | 189 | 167 | 0.212 | 0.052 |
| | 185 | 169 | 0.208 | 0.052 |

*End of table.*

**Table A.16:** Data for examination of the pediatric phantom, with 102 kV and a field size of 17 cm x 12.3 cm.

| mA | DAP w/ grid [mGycm$^2$] | DAP w/o grid [mGycm$^2$] | mAs w/ grid | mAs w/o grid | EI w/ grid | EI w/o grid |
|---|---|---|---|---|---|---|
| 50 | 7 | 3 | 0.4 | 0.25 | 161 | 212 |
| | 7 | 4 | 0.4 | 0.25 | 163 | 214 |
| | 6 | 4 | 0.4 | 0.25 | 162 | 222 |
| | 7 | 4 | 0.4 | 0.25 | 161 | 212 |
| | 7 | 5 | 0.4 | 0.25 | 163 | 214 |
| 25 | 5 | 3 | 0.3 | 0.175 | 127 | 157 |
| | 5 | 3 | 0.3 | 0.175 | 129 | 160 |
| | 6 | 2 | 0.325 | 0.175 | 137 | 159 |
| | 5 | 4 | 0.3 | 0.175 | 130 | 159 |
| | 5 | 2 | 0.3 | 0.175 | 129 | 159 |

**Table A.17:** Data for examination of the pediatric phantom (ms values) with 102 kV.

| mA | ms w/ grid | ms w/o grid |
|---|---|---|
| 50 | 8 | 5 |
| | 8 | 5 |
| | 8 | 5 |
| | 8 | 5 |
| | 8 | 5 |
| 25 | 12 | 7 |
| | 12 | 7 |
| | 13 | 7 |
| | 12 | 7 |
| | 12 | 7 |

**Table A.18:** The DAP for exposure on a 7 cm thick phantom, while covering none and half of the AEC with 1 mm lead, using 60 kV and 7.1 x 6.3 cm in field size.

| Coverage of the centre AEC ROI | DAP [mGycm$^2$] | EI | mAs |
|---|---|---|---|
| None | 1 | 173 | 0.65 |
| Half | 2 | 8 | 1 |

**Table A.19:** Calculation of error propagation for varying thickness of PMMA with DAP from exposures.

| Thickness | Mean DAP w/ grid | Mean DAP w/o grid | $\sigma_w$ with grid | $\sigma_{w/o}$ without grid | Mean $R$ | Uncertainty $\sigma$ |
|---|---|---|---|---|---|---|
| 10 | 14.6 | 4 | 0.245 | 0 | 3.65 | 0.061 |
| 12 | 22.6 | 5.6 | 0.245 | 0.245 | 4.036 | 0.182 |
| 15 | 42.4 | 9.8 | 0.678 | 0.2 | 4.3265 | 0.112 |
| 17 | 67 | 15.4 | 0.548 | 0.245 | 4.351 | 0.078 |
| 20 | 125.4 | 26.6 | 2.694 | 0.245 | 4.714 | 0.110 |
| 22 | 192 | 37.4 | 3.209 | 0.400 | 5.134 | 0.102 |
| 25 | 357.2 | 67.8 | 5.757 | 0.663 | 5.268 | 0.100 |
| 27 | 538.2 | 98.4 | 7.902 | 0.748 | 5.4695 | 0.090 |
| 30 | 1028.8 | 175 | 25.13 | 3.521 | 5.88 | 0.186 |

**Table A.20:** Calculation of error propagation for varying kV, for 10 cm of PMMA with DAP from exposures.

| kV | Mean DAP w/ grid | Mean DAP w/o grid | $\sigma_w$ with grid | $\sigma_{w/o}$ without grid | Mean $R$ | Uncertainty $\sigma$ |
|---|---|---|---|---|---|---|
| 50 | 51.4 | 13.6 | 0.245 | 0.4 | 3.780 | 0.113 |
| 60 | 31.6 | 7.8 | 0.4 | 0.2 | 4.051 | 0.116 |
| 70 | 20.6 | 5.6 | 0.245 | 0.245 | 3.679 | 0.167 |
| 80 | 13.8 | 4 | 0.374 | 0 | 3.45 | 0.094 |
| 90 | 11.6 | 4 | 0.245 | 0 | 2.9 | 0.061 |
| 100 | 10.6 | 4.4 | 0.245 | 0.245 | 2.409 | 0.145 |
| 110 | 11.4 | 5 | 0.245 | 0 | 2.28 | 0.049 |
| 120 | 11.4 | 5.2 | 0.245 | 0.2 | 2.192 | 0.097 |
| 130 | 10.8 | 5.6 | 0.2 | 0.245 | 1.929 | 0.091 |

**Table A.21:** Calculation of error propagation for varying kV, for 15 cm of PMMA with DAP from exposures.

| kV | Mean DAP w/ grid | Mean DAP w/o grid | $\sigma_w$ with grid | $\sigma_{w/o}$ without grid | Mean $R$ | Uncertainty $\sigma$ |
|---|---|---|---|---|---|---|
| 50 | 180 | 41 | 6 | 1 | 4.39 | 0.181 |
| 60 | 102.5 | 22.5 | 0.5 | 0.5 | 4.56 | 0.104 |
| 70 | 65 | 15 | 0.894 | 0.316 | 4.33 | 0.110 |
| 80 | 44.2 | 9.6 | 0.97 | 0.245 | 4.604 | 0.155 |
| 90 | 34.4 | 8 | 0.40 | 0 | 4.3 | 0.05 |
| 100 | 32.8 | 8 | 0.490 | 0 | 4.1 | 0.061 |
| 110 | 32.2 | 8.4 | 0.374 | 0.245 | 3.83 | 0.120 |
| 120 | 29.4 | 8 | 0.510 | 0 | 3.675 | 0.064 |
| 130 | 25.4 | 8 | 0.678 | 0 | 3.175 | 0.085 |

**Table A.22:** Calculation of error propagation for varying kV, for 20 cm of PMMA with DAP from exposures.

| kV | Mean DAP w/ grid | Mean DAP w/o grid | $\sigma_w$ with grid | $\sigma_{w/o}$ without grid | Mean $R$ | Uncertainty $\sigma$ |
|---|---|---|---|---|---|---|
| 70 | 198 | 38.5 | 2 | 0.5 | 5.143 | 0.085 |
| 80 | 131.2 | 26.8 | 1.828 | 0.663 | 4.90 | 0.140 |
| 90 | 100.6 | 20.6 | 1.4 | 0.4 | 4.8835 | 0.117 |
| 100 | 94 | 19 | 1.517 | 0.447 | 4.948 | 0.141 |
| 110 | 91.2 | 18.2 | 1.772 | 0.2 | 5.011 | 0.112 |
| 120 | 82 | 16.4 | 2.280 | 0.510 | 5 | 0.209 |
| 130 | 72.4 | 15.8 | 1.208 | 0.374 | 4.583 | 0.133 |

**Table A.23:** Calculation of error propagation for varying kV, for 25 cm of PMMA with DAP from exposures.

| kV | Mean DAP w/ grid | Mean DAP w/o grid | $\sigma_w$ with grid | $\sigma_{w/o}$ without grid | Mean $R$ | Uncertainty $\sigma$ |
|---|---|---|---|---|---|---|
| 80 | 387.6 | 70.4 | 7.239 | 1.844 | 5.506 | 0.177 |
| 90 | 288.6 | 54.8 | 6.957 | 1.360 | 5.267 | 0.182 |
| 100 | 259 | 49.6 | 7.124 | 0.3873 | 5.222 | 0.15 |
| 110 | 244 | 46.6 | 6.14 | 0.949 | 5.23 | 0.17 |
| 120 | 210.2 | 41.8 | 2.757 | 0.922 | 5.029 | 0.13 |
| 130 | 194.6 | 37.4 | 1.844 | 0.633 | 5.203 | 0.101 |

**Table A.24:** Calculation of error propagation for varying kV, for 30 cm of PMMA with DAP from exposures.

| kV | Mean DAP w/ grid | Mean DAP w/o grid | $\sigma_w$ with grid | $\sigma_{w/0}$ without grid | Mean $R$ | Uncertainty $\sigma$ |
|---|---|---|---|---|---|---|
| 80 | 1095 | 177.6 | 59.99 | 8.58 | 6.17 | 0.45 |
| 90 | 766.2 | 132.8 | 23.29 | 5.11 | 5.77 | 0.283 |
| 100 | 663.8 | 119.4 | 23.28 | 5.604 | 5.56 | 0.326 |
| 110 | 618.6 | 112.2 | 16.78 | 2.31 | 5.514 | 0.188 |
| 120 | 539.2 | 96 | 19.61 | 1.94 | 5.62 | 0.234 |
| 130 | 469.8 | 85.2 | 14.03 | 2.89 | 5.514 | 0.25 |

**Table A.25:** Calculation of error propagation for varying field size on PMMA with DAP from exposures.

| kV | Mean DAP w/ grid | Mean DAP w/o grid | $\sigma_w$ with grid | $\sigma_{w/o}$ without grid | Mean $R$ | Uncertainty $\sigma$ |
|---|---|---|---|---|---|---|
| 15 | 124 | 30.8 | 1.66 | 0.592 | 4.026 | 0.095 |
| 17.3 | 154.2 | 34.6 | 3.06 | 1.285 | 4.457 | 0.188 |
| 20 | 197 | 39.8 | 3.640 | 0.775 | 4.95 | 0.133 |
| 22.3 | 231.8 | 43.8 | 3.332 | 0.775 | 5.292 | 0.121 |
| 25 | 284 | 49 | 5.5 | 0.5 | 5.796 | 0.127 |
| 27.3 | 327.2 | 52.4 | 7.49 | 1.072 | 6.245 | 0.192 |
| 30 | 383.2 | 58.6 | 5.621 | 1.38 | 6.540 | 0.181 |
| 32.3 | 435.4 | 63.8 | 6.975 | 0.922 | 6.825 | 0.147 |
| 35 | 502.2 | 70 | 8.298 | 1.73 | 7.174 | 0.21 |

**Table A.26:** Calculation of error propagation for the AP chest phantom examination with DAP from exposures.

| Thickness | Mean DAP w/ grid | Mean DAP w/o grid | $\sigma_w$ with grid | $\sigma_{w/o}$ without grid | Mean $R$ | Uncertainty $\sigma$ |
|---|---|---|---|---|---|---|
| 21 | 45.2 | 25.4 | 0.583 | 0.68 | 1.78 | 0.053 |
| 27 | 83.2 | 39 | 0.2 | 0.316 | 2.13 | 0.018 |
| 32 | 202.6 | 80.8 | 0.51 | 2.311 | 2.507 | 0.072 |

**Table A.27:** Calculation of error propagation for AP chest phantom examination with DAP from exposures.

| Field size [cm x cm] | Mean DAP w/ grid | Mean DAP w/o grid | $\sigma_w$ with grid | $\sigma_{w/o}$ without grid | Mean $R$ | Uncertainty $\sigma$ |
|---|---|---|---|---|---|---|
| 41.4 x 39.5 * | 298 | 107 | 0.55 | 0.316 | 2.79 | 0.01 |
| 30.9 x 36.5 ** | 195.8 | 78.8 | 0.8 | 0.2 | 2.485 | 0.012 |

* 125 kV ** 141 kV

**Table A.28:** Calculation of error propagation for LAT chest phantom examination with a field size of 19.2 cm x 16 cm, with DAP from exposures.

| Thickness | Mean DAP w/ grid | Mean DAP w/o grid | $\sigma_w$ with grid | $\sigma_{w/o}$ without grid | Mean $R$ | Uncertainty $\sigma$ |
|---|---|---|---|---|---|---|
| 29 | 10.6 | 5.6 | 0.245 | 0.245 | 1.893 | 0.094 |
| 35 | 22.2 | 10.4 | 0.2 | 0.245 | 2.135 | 0.054 |
| 39 | 36.6 | 15.4 | 0.4 | 0.4 | 2.376 | 0.067 |
| 39* | 70.8 | 28.8 | 0.374 | 0.2 | 2.458 | 0.0215 |

* Field size of 24.3 cm x 26 cm.

**Table A.29:** Calculation of error propagation for the pelvis phantom examination with DAP from exposures.

| Thickness | Mean DAP w/ grid | Mean DAP w/o grid | $\sigma_w$ with grid | $\sigma_{w/o}$ without grid | Mean $R$ | Uncertainty $\sigma$ |
|---|---|---|---|---|---|---|
| 23 | 641.6 | 141 | 2.074 | 0.7071 | 4.55 | 0.027 |
| 29 | 570 | 103.8 | 4.690 | 0.836 | 5.491 | 0.063 |
| 35 | 1842.6 | 283.4 | 43.35 | 4.561 | 6.502 | 0.185 |
| 35* | 836 | 157.2 | 15.248 | 1.643 | 5.32 | 0.112 |

* 85 kV.

**Table A.30:** Calculation of error propagation for the hip phantom examination with DAP from exposures.

| Thickness | Mean DAP w/ grid | Mean DAP w/o grid | $\sigma_w$ with grid | $\sigma_{w/o}$ without grid | Mean $R$ | Uncertainty $\sigma$ |
|---|---|---|---|---|---|---|
| 23 | 189.4 | 51.4 | 3.286 | 0.895 | 3.685 | 0.091 |
| 29 | 703 | 151.4 | 9.19 | 4.51 | 4.643 | 0.151 |
| 35 | 1051.2 | 255 | 8.87 | 1 | 4.12 | 0.038 |

**Table A.31:** Calculation of error propagation for the pediatric phantom examination with DAP from exposures.

| Mean DAP w/ grid | Mean DAP w/o grid | $\sigma_w$ with grid | $\sigma_{w/o}$ without grid | Mean $R$ | Uncertainty $\sigma$ |
|---|---|---|---|---|---|
| 6.8 | 4 | 0.447 | 0.707 | 1.70 | 0.32 |
| 5.2 | 2.8 | 0.45 | 0.837 | 1.857 | 0.578 |


UNIVERSITY OF
GOTHENBURG